TÉCNICO LISBOA

# Microfluidic preparation of alginate microparticles for targeted delivery

**Christian Leonardo Riera Orozco**

Thesis to obtain the Master of Science Degree in

## Chemical Engineering

Supervisor(s):
Prof. Dr. Pedro Carlos De Barros Fernandes (IST)
Prof.Dr[a] Viola Tokárová (UCT)

### Examination Committee

Chairperson: Prof. Dr. Mário Nuno de Matos Sequeira Berberan e Santoso
Supervisor: Dr. Pedro Carlos de Barros Fernandes
Member of the Committee: Prof. Dr. Ana Catarina Beco Pinto Reis

**December 2020**

I declare that this document is an original work of my own authorship and that it fulfills all the requirements of the Code of Conduct and Good Practices of the Universidade de Lisboa.

# Acknowledgments

First of all, I would like to thank my parents, who instilled and taught me to prioritize study above all. Apart from a good example of self-improvement, they always managed to create an environment conducive to study, even in the most difficult moments. The example they gave me and the support they gave me was fundamental throughout my academic life.

To my brother, for helping me with everything I needed and for giving me a football moment every weekend with which I could de-stress a bit. Contributing to his personal and academic development was always a source of inspiration and self-improvement.

This thesis is also dedicated to my grandmother, rest in peace, who took the first step so that today I can be presenting this thesis. I will never forget a phrase that she said and since then I have had it as a premise for my future life - ”A shovel weighs more than a pen”.

Also, to my university and Erasmus colleagues, thanks to them my university life was full of unforgettable moments, emotions and experiences. Specially to Karolina, for the shared moments, discover of a new world, for being with me in those moments when work occupied my time and for changing my way of thinking to the point of making one of the most important decisions of my life.

To professor Viola Tokarová,phD for giving me the opportunity to learn more about the Laboratory of Biomimetic Engineering, for accepting me for internships and for giving me enough autonomy to investigate by my own, but at the same time guiding me when I needed.

To professor Pedro Fernandes, phD for using his experience in the area to help me with more technical issues and advise me at various times during the last months. Everything you provide me was essential to this thesis.

And to all the UCT students and researchers who contributed to my work. For their advices, assistance, and for always having time to help me.

# Abstract

Whether termed micro-total analysis systems, lab-on-a-chip, or microfluidic devices, the technologies that define the field of microfluidics have shown great promise for overcoming many challenges in environmental, clinical, chemical and biological analyses.

The objective of this work was to produce microparticles of alginate containing iron oxide nanoparticles that increase the ease of manipulation of the particles. After, the particles surface was modified to give copolymer properties to the particles and thus be able to assign properties necessary for each situation or to transport substances through targeted delivery. The size of each particle was measured and compared to obtain a mathematical model that can predict the particles sizes for different flow rates.

A flow focusing cross junction microfluidics reactor was designed in PDMS which can control the size of microparticles by adjusting the flow rate of inlets.

This approach offers a potentially lower cost, adjustable process for making microparticle compared to other more traditional polymerization approaches.

Computational models can also help to produce pressure droplet correlations. In this work, COMSOL Multiphysics was used to contribute to the determination of how the fluid behave in the junction and how the particles is produced.

**Keywords:** Microfluidics, alginate, undecanol, targeted delivery, COMSOL multiphysics

# Resumo

Quer sejam denominados sistemas de análise micro-total, lab-on-a-chip ou dispositivos microfluídicos, a tecnologias que definem o campo dos microfluidos têm mostrado grande promessa para a superação muitos desafios em análises ambientais, clínicas, químicas e biológicas.

O objetivo de este trabalho foi produzir micropartículas de alginato contendo nanopartículas de óxido de ferro, que aumentam a facilidade de manipulação das partículas. Depois, a superfície das partículas foi modificada para dar propriedades de copolímero às partículas e, assim, ser capaz de atribuir propriedades necessárias para cada situação ou para transportar substâncias por meio de administração orientada. O tamanho de cada partícula foi medido e comparado para obter um modelo matemático que pode prever os tamanhos das partículas para diferentes taxas de fluxo.

Uma reator microfluídico *flow focusing* com junção cruzada foi esboçado em PDMS, que pode controlar o tamanho das micropartículas, ajustando a taxa de fluxo das entradas.

Essa abordagem oferece um custo potencialmente mais baixo, processo ajustável para fazer micropartículas em comparação com outros mais tradicionais abordagens de polimerização.

Modelos computacionais também podem ajudar a produzir correlações de gota de pressão. Neste trabalho, o COMSOL Multiphysics foi utilizado para determinar a forma como o fluido se comporta na junção e como as partículas são produzidas.

**Keywords:** Microfluidos, alginato, undecanol, libertação controlada de fármacos, COMSOL multiphysics.

# Contents

# List of Tables

# List of Figures

# Nomenclature

**Symbols**

| | |
|---|---|
| $\eta$ | dynamic viscosity |
| $\lambda$ | viscosity ratio |
| $\Phi$ | flow rate ratio |
| $\phi_s$ | association parameter |
| $\rho$ | density of fluid |
| $\sigma$ | surface tension |
| $\theta$ | contact angle |
| ABIL | cetyl PEG/PPG-10/1 Dimethicone Triglyceride |
| B | Bond number |
| Ca | capillary number |
| D | diameter of tube |
| d | diameter of particle |
| $D_f$ | diffusion coefficient |
| E | energy |
| FFL | fick's First Law |
| J | mass flow per unit of area |
| L | characteristic length |
| LCST | lower critical solution temperature |
| $M_s$ | molecular weight |
| O/W | oil-in-water |
| OMTS | octamethyltrisiloxane |
| PDMS | polydimethylsiloxane |
| PEGDA | poly(ethylene glycol) diacrylate |
| PMMA | poly(methyl methacrylate) |

PNIPAAm poly(N-isopropylacrylamide)

PS polystyrene

Q flow rate

r radius of particle

Re Reynolds number

T temperature

TPF two phases flow

u flow speed

$V_D$ molar volume

W/O water-in-oil

We Weber number

# Chapter 1

# Introduction

Throughout the last century miniaturization has played a crucial role in modern technology and revolutionized society. Great advances has been made in both technology (micro- and nanotechnology), but also within the fields of chemistry and biology, where improvements in optical systems has opened a world of new possibilities.

In the early 1990's, a new field of science begun around the inkjet printer manufacturing. The mechanism behind these printers is based on microfluidics; it involves the use of very small tubes carrying the ink for printing [1].

Microfluidics is the science of manipulating and controlling fluids, usually in the range of microliters ($10^{-6}$) to picoliters ($10^{-12}$), in networks of channels with dimensions from tens to hundreds of micrometers [2]. At this scale, researchers can take advantage of the scaling of many physical laws and employ, for example, rapid diffusion, laminar flows, dean flow, rapid thermal transport, and take advantage of the large surface area relative to the volume [3].

So microfluidics seems almost too good to be true: it offers so many advantages and so few disadvantages (at least in its major applications in analysis). In fact, concerning the time and circumstances required for microfluidics to develop into a major new technology are important not just for this field, but also for other new technologies struggling to make it into the big time. Empowered by the versatile microfabrication technologies that have stemmed from the technologies used for microelectronics and microelectromechanical systems (MEMS), microfluidics offers salient advantages over conventional platforms, such as high resolution and sensitivity in separation and detection, lower cost for fabrication than laboratorial or industrial devices, low sample consumption and low waste, short time for analysis, and small device footprint.

The development of microfluidics has just begun. A number of factors suggest that there are many early-stage applications of microsystems containing fluids, including the exploration of fluidic optics and cells, the development of new types of organic synthesis in small-channel systems, the continuing development of technologies based on large arrays of detectors and on high-throughput screening, the fabrication of microrobotic systems using hydraulic systems based on microfluidics, other fluidic versions of MEMS, and work on biomimetic systems with microfluidic components [4].

# Chapter 2

# Microfluidics

Droplet microfluidics is one of the most important subcategories of microfluidics, which creates and manipulates discrete droplets through immiscible multiphase flows inside microchannels. Droplet microfluidics mainly refers to chip fabrication, droplet formation, manipulation and applications. Among all microfluidic systems, those intended for the generation of microdroplets have inspired many researchers and led to various innovations for different applications, attributed to the following advantages: a small volume of reagents consumed, massive production of monodisperse droplets, high surface-area-to-volume ratio that facilitates fast reaction, and independent control of each droplet.

In general, applications of microfluidic droplets arise from two distinct but complementary aspects. One exploits droplets with well-defined components and structures as templates in materials science, for example, synthesis of microcapsules, microparticles, and microfibers applicable to pharmaceuticals, cosmetics, medical and foods; another involves lab-on-a-chip applications where droplets are used as microreactors to perform chemical and biochemical reactions. In most of these applications, highly uniform predictable outcomes.

## 2.1 Passive microfluidic

In order for droplet formation to occur, two immiscible phases, referred to as the continuous phase (medium in which droplets are generated) and dispersed phase (the droplet phase), must be used. In passive microfluidics, droplets generation originates from fluid instabilities. The size of the generated droplets is mainly controlled by the flow rate ratio of the continuous phase and dispersed phase, interfacial tension between two phases, and the geometry of the channels used for droplet generation. The passive microfluidics devices have one of these five modes Figure 2.1: squeezing, dripping, jetting, tip-streaming and tip-multi-breaking.

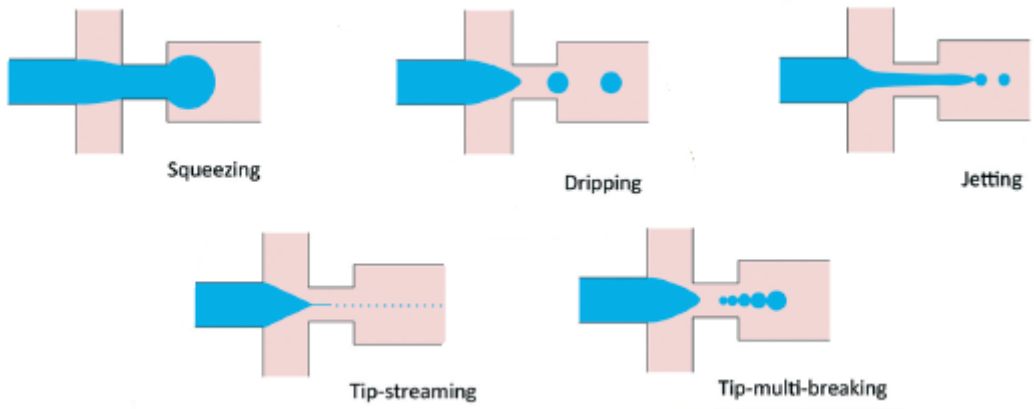


Figure 2.1: Representation of microfluidics juntions for passive droplet formation. [5]

The squeezing arises from a quite different mechanism from the capillary (Rayleigh–Plateau) instability that is responsible for the other four modes. Channel confinement plays a dominant role in the squeezing regime and inhibits capillary instability so that breakup exhibits quasi-static mechanisms until the last stage of thread pinch-off. The other four modes of breakup come from the capillary instability as interfacial tension forces seek to minimize the interfacial area according to the thermodynamic principle of minimum interfacial energy. In these cases, viscous and inertial forces that act to deform the liquid interface counteract interfacial tension forces that resist the deformation. It is the competition of these forces that determines the specific breakup mode of droplet generation for a given set of parameters [5].

## 2.2 Active microfluidics

The precision manipulation of streams of fluids with microfluidic devices is revolutionizing many fluid-based technologies and enabling the development of high-throughput reactors that use minute quantities of reagents. However, there are some drawbacks in passive control such as the contamination effects due to surface adsorption and diffusion limit the smallest quantities that can be used or the slow response time in the order of seconds or even minutes. The long response time comes from the relatively large fluidic resistance of the tubing and the fluidic capacitance caused by the compressibility of the liquid or the channel material.

Active techniques add another level of controllability in modulating droplet formation with the aid of additional energy input by external elements in addition to the pressure applied typically through a syringe pump in passive techniques. Some of the most used ways of adding energy to a microfluidic system are electrical, thermal, magnetic and mechanical (Figure 2.2).

Electric energy can be used to manipulate droplet generation. By combining electrostatic charge on the droplets and electric fields on the devices, is possible to develop modules that create, recombine, split, and sort droplets one by one, thus providing fine control over individual microreactors while retaining high purity and enabling very high throughput. By incorporating the forces that result from charging the aqueous fluid in an electric field E, smaller droplets can be produced with more precise control of their individual timing than is feasible with other strategies that rely solely on viscous forces to overcome surface tension [6].

Thermal control of droplet generation can be categorized into two approaches according to the way the heat is introduced. The first approach utilizes resistive heating at the junction where the droplets are formed. The temperature is controlled by the applied current and feedback from a temperature

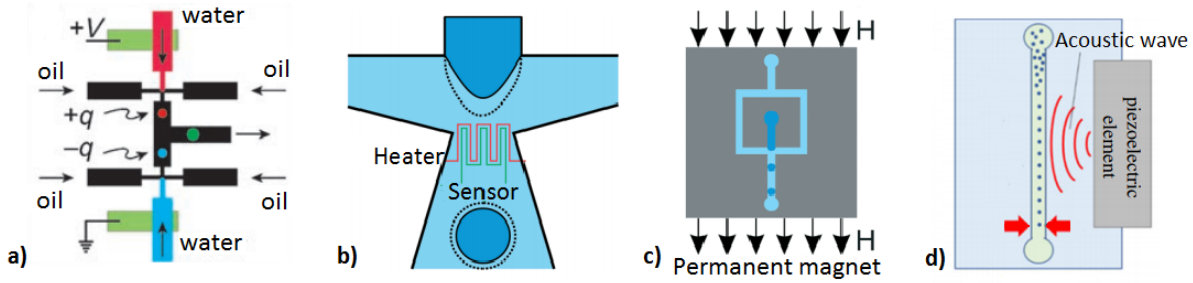


Figure 2.2: Different types of active microfluidics a) Electrical microfluidics b) Thermal microfluidics c) Magnetic microfluidic d) Piezoelectric microfluidics (mechanical)

sensor. The second approach utilizes a focused laser beam to achieve localized heating. Thermal control of droplet generation can be categorized into two approaches according to the way the heat is introduced. Thermal control is based on the temperature dependency of the fluid properties, mainly the viscosity and interfacial tension. For most fluids, viscosity and interfacial tension decrease with increasing temperature. This change is reflected in the change in capillary number Ca [7].

Magnetic manipulation of microfluids is an attractive concept. Due to the non-invasive nature of magnetic fields, magnetic particles or magnetic fluids can be manipulated inside a microfluidic channel by external magnets that are not in direct contact with the fluid. Ferrofluids are stable colloid suspensions of magnetic microparticles such as magnetite, maghemite or cobalt ferrite dispersed in a base fluid, such as water or organic solvent. External magnetic fields can be applied to control their fluid motion and their fluidic properties are retained even under the influence of strong magnetic fields. Ferrofluids can move just as single component fluids thorough microchannels of microfluidic devices [8]. The interparticle magnetic energy in a ferrofluid is weak because of the small particle size of less than 10 nm and the surfactant coating. Thus, thermal energy can overcome magnetic potential and evenly distributes the magnetic particles by Brownian motion .

Mechanical control of droplet generation involves physical deformation of the liquid interface using hydraulic, pneumatic or piezoelectric actuation. Hydraulic and pneumatic actuations are usually executed by valves integrated into the microfluidic devices. Generally, the valves are made of the same elastic device material such as PDMS. The valves are actuated pneumatically using compressed air or hydraulically by applying pressure to the liquid filled valve chamber.The piezoelectric actuator accurately converts electric voltage into mechanical translation which directly determines the volume of the fluid segment. The control approaches can be categorized according to the function of the piezoelectric element. For dispensing purposes, a piezoelectric actuator can be used to supply a fixed amount of dispersed phase for on-demand droplet generation as in ink-jet printing applications. On the other hand, piezoelectric actuation can disturb the interface between continuous and dispersed phases and affect the droplet generation process. Compared to the previously mentioned on-demand droplet generation approaches using pneumatic/hydraulic actuation, piezoelectric actuation is faster. While pneumatic/hydraulic actuation allows for 40 ms dispensing time, piezoelectric actuation can achieve 200 $\mu$s [7].

## 2.3 Dimensionless numbers

In the world of small scale, surface area to volume ratio ($r_{sv}=\frac{S}{V}$) becomes bigger, due to their units. Something similar happen to molecular forces and charge distributions across a molecule. To understand when fluids will respond to bulk forces vs molecular-molecular forces, some dimensionless numbers help to determine which would be the behaviour of the system. There are a lot of numbers to

consider, but we will focus on those that will apply to our project. Those numbers are reynolds number, capillary number, weber number, bond number, viscosity ratio and flow rate ratio (Table 2.1) [9].

Table 2.1: Dimensionless parameters in microfluidic droplet generation.

| Symbol | Name | Formula | Physical meaning |
|---|---|---|---|
| Re | Reynolds number | $Re = \frac{\rho u D}{\eta}$ | Inertial force/viscous force |
| Ca | Capillary number | $Ca = \frac{\mu u}{\sigma}$ | Viscous force/interfacial tension |
| We | Weber number | $We = \frac{\rho u^2 L}{\gamma}$ | Inertial force/interfacial tension |
| Bo | Bond number | $Bo = \frac{\Delta \rho g L^2}{\sigma}$ | Buoyancy/interfacial tension |
| $\lambda$ | Viscosity ratio | $\lambda = \frac{\eta_d}{\eta_c}$ | Dispersed viscosity/continuous viscosity |
| $\phi$ | Flow rate ratio | $\phi = \frac{Q_d}{Q_c}$ | Dispersed flow rate/continuous flow rate |

Reynold's number describes the boundary between viscous and inertial flow, how much molecules stick together because of inter molecular forces and how much the fluid will flow with the bulk due to velocity of the flow. When molecular forces overcome bulk flow, laminar flow, that is flow without turbulence, two adjacent fluids simply don't mix as each fluid moves in undisrupted, parallel layers. Molecules in the flow carry on in a straight path, while molecules overwhelmed by molecular forces are often slowed by the attraction to the channel walls [9]. Very few microfluidic systems use turbulent flows. It is recalled that, in enclosures, a number of Reynolds of 2,000 is required to reach the transition to turbulence.

Capillary number (Ca) describes the boundary between viscous and interfacial forces. The interfacial force appears between the wall and the fluid or between two immiscible fluids (a pattern that is taken advantage of in droplet microfluidics), The viscous forces, preventing flow, are between the molecules within the fluid. We use this property to move fluids throughout the device without pumps. The fluid can be attracted to move because the surface of the channel is more chemically or electrically compatible than the viscous forces between the fluid molecules. As the fluid molecules creep at the fluid front, the adjacent molecules are pulled along due to viscous forces. Generally motion happens at Ca about 1 or less [9].

Weber number relates the inertia forces to the forces resulting from surface tension. When a liquid flows through a second fluid phase (gas or liquid), then the fluid-mechanical or aerodynamic force causes the drops to deform and ultimately disperse. If the deforming force increases due to a higher speed

or longer process length, the drops of a spray disperse more easily and drops of oil in an aqueous environment are split apart more easily. A high surface or interfacial tension counteracts this process. Surfactants, which reduce the surface tension of the liquid or the interfacial tension between the phases concerned, are therefore often used in sprays and emulsions. The same applies to extraction processes in which small droplets must ensure a large exchange surface area at the phase boundary [10].

Bond number characterizes the ratio of gravitational forces to surface or interfacial tension forces. A value of Bo $<<1$ implies the flow in question is only weakly dependent on gravitational forces, whereas Bo $>>1$ implies gravitational forces dominate over interfacial forces [11]. When it's close to one, both forces are similar. It may be derived in a number of ways, such as scaling the pressure of a drop of liquid on a solid surface or predict if water will climb up the walls of a tube because of cohesion between the wall and the fluid.

## 2.4 Microchip preparation

### 2.4.1 Microchip geometry

Several microfluific devices geometries might be taken in account, such as cross-flow, co-flow, flow focusing, step emulsification, microchanel emulsification and membrane emulsification [12]. Among them, the most common geometries are the cross-flow, co-flow and the flow focusing geometries (Figure 2.3.

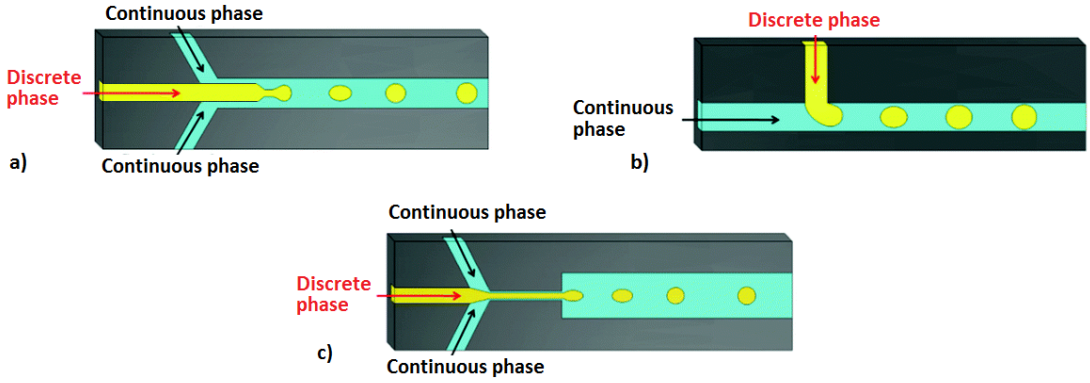


Figure 2.3: Different geometries for microfluidics devices: a) Cross-flow b) Co-flow c) flow focusing. [13]

In co-flow drop formation, the dispersed phase is injected through a small capillary centred within a larger capillary, flowing parallel to the flow of the continuous phase. Droplets are generated by the viscous shear of the continuous phase over the dispersed phase in a process that resembles a dripping faucet; as the emerging droplet grows, the viscous drag of the continuous phase increases. This continues until the drag is equal to the interfacial tension force adhering the base of the droplet to the capillary tip, at which point a droplet buds off and is carried downstream. In co-flow drop formation, the flows are 'unconfined' in the sense that the outer capillary is much larger than the inner capillary and the droplets that are formed; consequently, the drop formation mechanism depends mainly on viscous shear and surface tension, and interactions with the outer capillary wall can be neglected. A disadvantage of this geometry is that it is difficult to fabricate with lithographic processes because it requires the inner capillary to be smaller than, and nested within, the outer capillary [14].

In a T-junction (cross-flow) configuration, two phases (continuous and dispersed phase) are brought

into the system by externally controlled devices (usually pressure or syringe pump). In this configuration, the dispersed phase is pumped into the continuous phase orthogonally. As the dispersed phase enters the continuous, shear forces elongate the head of the dispersed phase until a segment eventually separates and relaxes into a sphere or plug shape due to interfacial tension [15]. The mechanism by which monodisperse drops are formed depends on the capillary number (Ca) of the flow. At higher capillary number, the large viscous drag of the continuous phase shears the droplets of the dispersed phase of the input channel. A characteristic of the drops formed by this mechanism is that they are smaller than the channel. A characteristic of drops formed by this mechanism is that they are smaller than the channel. Alternatively, at low Ca drops can also be produced through a mechanism squeezing.

Another drop formation geometry is the flow focus device. In this geometry, the dispersed phase is introduced from one channel and the continuous phase from channels on either side. The fluids are focused through an 'orifice,' where droplets are formed. There are several variations on this geometry, including one in which a small constriction is added at the orifice, as pictured in Figure 2.3, and in which the constriction is omitted, yielding a straight 'throat.' Both variations tend to form droplets with comparable properties for the majority of flow rates [14].

### 2.4.2 Material for microfluidics devices

In the early days of microfluidics research, devices were most commonly fabricated in silicon or glass and extend in only a few square centimeters in size. Glass in particular was seen as a good choice since it is optically transparent and electrically insulating, as well as being an amorphous material.

#### 2.4.2.1 Silicon

Silicon was among the first materials elected in the fabrication of microfluidics devices. They provide high precision, robustness and optical clarity. However, chip fabrication is costly (around 500 USD per chip) and in practice, devices are not heavily reused. In addition, it requires real expertise in microfabrication and a clean room. Nevertheless, it allows to achieve high precision silicon machining. Silicons have good surface stability, chemical compatibility and electrical conductivity which allows to integrate electronics on the microfluidic chip [16].

#### 2.4.2.2 Glass

Glass is another material that was used early in microfluidic chip manufacturing. It benefits from the same surface stability, thermal conductivity, and solvent compatibility properties of silicon. Moreover, glass is biocompatible, chemically inert, hydrophilic and allows efficient coatings. Its surface chemistry, superior optical transparency and high-pressure resistance make it the best choice for many applications. Some requirements for the glass used in microsystem technology are: microstructurable using standard lithography process, suitable for metal deposition, transparent for wide range of wavelength, apt for bonding to silicon. The main drawback of glass in microfluidic chips is its high cost [16].

#### 2.4.2.3 Polymer

Nowadays new techniques are used now to prototype and produce microfluidic chips and provides a much wider range of material choices. Polymers have fast become more viable materials than silicon or glass since they exhibit excellent material properties while also being less expensive both in purchase price and cost of processing. In particular, the most commonly used for microfluidic chips is polydimethylsiloxane (PDMS), owing to its price and rapid prototyping.

Poly(methyl methacrylate) (PMMA) is a rigid thermoplastic material that has an optical transparency in visible light wavelengths. Is an inexpensive polymer that has become one of the most commonly used materials in microfluidic systems. Despite its low price, it exhibits the properties needed to fabricate good quality devices. The polymer is also compatible with electrophoresis, which is important for many types of research [17]. This polymer also features others properties such as its ease of fabrication and modification

Poly(ethylene glycol) diacrylate (PEGDA) have some useful properties such as water stability, optical clarity and low background fluorescence. However, it shows less nonspecific adsorption and has greater resistance to permeation of small hydrophobic molecules than other materials. This polymer could be considered as a convenient material since polymerization can occur rapidly at room temperature and doesn't require too much energy. PEGDA can be used to build robust microfluidic valves and pumps in different shapes for application in small volume assays. Due to its resistance to nonspecific adsorption, PEGDA can have broad use in small volume analysis and biomedical research since it is a biocompatible polymer [18].

Polystyrene (PS) is optically transparent, biocompatible, inert, rigid, and its surface can be easily functionalized[61]. Its hydrophobic surface can be made hydrophilic by various physical and chemical means including corona-discharge, gas plasma, and irradiation[62]. However, the necessity of expensive equipment required to realize complex chips from such polymer (injection molding, hot embossing) could be a hindrance for its use. PS is adapted to mass manufacturing processes, thus it could facilitates translation of currently used manufacturing process to microscale systems. Some PS microfluidic chips take advantage of the shrinkage properties of thermoplastic PS sheets. In fact, after heating, etched microfluidic channels become thinner and deeper than the tooling[64]. Faster than soft lithography, this technique includes a simultaneous rapid bonding step, and complex PS multi-layered microchips can thus be completed in a matter of minutes [18].

Polydimethylsiloxane (PDMS) is hailed as one of the foundational materials for microfluidics. The silicone-based elastomer have many desirable properties, such as hydrophobicity and viscoelasticity. The loading and unloading of a stress-strain curve for PDMS do not coincide; rather, the amount of stress will vary based on the degree of strain, and the general rule is that increasing strain will result in greater stiffness. When the load itself is removed, the strain is slowly recovered. The procedure for fabricating such microchips is based on soft lithography, involving photolithography steps for producing a mold. If PDMS is left on a surface for long time, it will flow to cover the surface and mold the surface lithography. Cured with a cross-linking agent is possible to obtain a permanent deformation. Then bonding the PDMS slab to a glass slide or PDMS surface to seal the microchannels. In this way, it is possible to cast several PDMS replicas using the same mold.

A PDMS microchip, which has microchannels for electrophoretic separation, can be easily fabricated through microscale molding processes. For laboratory use, a silicon wafer with patterned photoresist can be used as a mold master. PDMS can replicate fine structures down to a submicron feature size. It easily get microstructures with smooth surfaces. In most biochemical analysis, fluorescent dyes are widely used for detection and quantification of molecules. PDMS has favorable mechanical and optical properties for a fluorescence-based detection scheme as shown in Figure 2.4 and Figure 2.5, respectively. The PDMS prepared with mixing ratio of base polymer to curing agent of 5 to 1, presents a high failure point and resistance for high pressures.On the other hand, it has almost no absorbance in the range of visible wavelength. Another attractive feature of PDMS as a material of microchip is its spontaneous adhesion onto flat surfaces. Generally, microfluidic devices have a confined microchannels and microchambers, which are realized by elaborate bonding processes, for instance, fusion bonding method for glass substrates and anodic bonding method for silicon–glass bonding. But in the case of PDMS, the microstructure can be sealed by just pasting the chip onto a flat substrate [20].

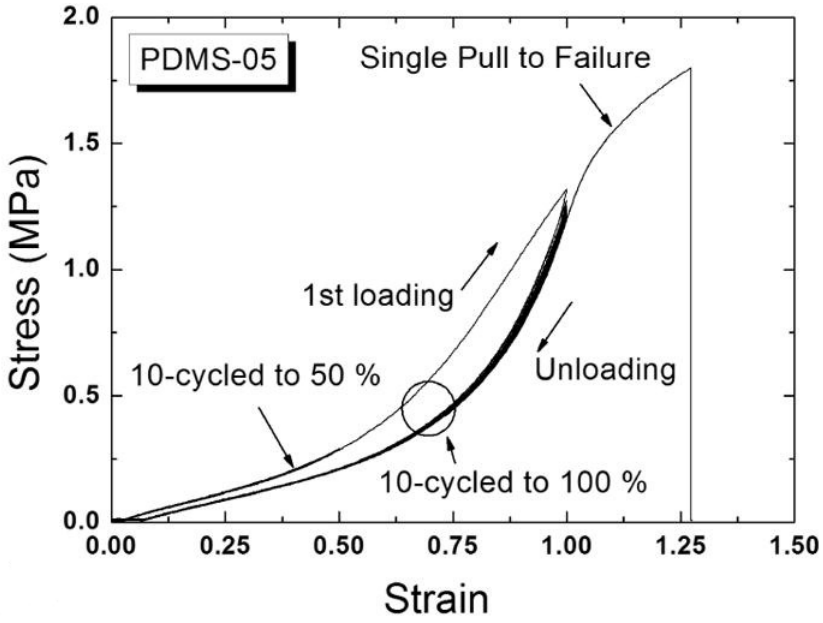


Figure 2.4: Strain–stress curves of PDMS with loading and unloading behaviour. [19]

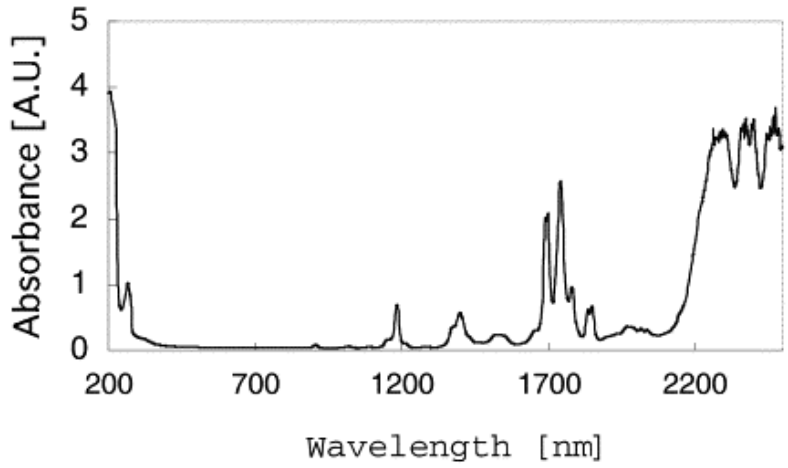


Figure 2.5: Graphical representation of the optical properties of PDMS. [20]

## 2.5 Oil in microfluidics

In recent years, the water-in-oil (W/O) system because of its appropriate physical properties has been mainly used to generate aqueous droplets in an oil environment [21]. Due to their polarity oil and water do not mix, but often they are made to mix in the form of emulsions by dispersing either component as fine droplets in the other. Emulsions are widely used in such industries as food, pharmaceutical, cosmetic, chemical, agricultural, print/ink, and petroleum. In recent years, considerable interest has emerged in emulsions containing droplets in the size range of micro and nanometers. Such emulsions (micro/nanoemulsions), differ from macroemulsions in several aspects. Owing to the small droplet size, this emaulsions are transparent or translucent, and creaming or sedimentation is significantly slower. The small droplet size also has potential benefits for developing a new realm of applications such as pharmaceutical and cosmetic formulations, as well as reactors for synthesizing small scale material.

Companies like Abbott and Opko are based on microfluidics operation and their application.

One of the commonly used platforms for droplet-based microfluidics is based on devices with closed microchannels. Discrete droplets are then produced in a continuously flowing immiscible liquid, and manipulated by downstream changes in the flow.

Effective utilization of the possibilities offered by the droplet-based two-phase flow (TPF) platform, also requires tuning the chemistry and physics of the device (and its operation) to that of the application. For example, where chemistry enters the picture concerns the wettability of the inner surfaces of the microfluidic chip. The continuous phase should wet the channel surface favorably, whereas the dispersed phase should be disfavored by the channel walls. For instance, hydrophobic channels need hydrophobic continuous phase, whereas hydrophilic channels require oil-in-water emulsions.

Very hydrophilic or very hydrophobic particles make poor emulsions unstable to coalescence, whereas particles of intermediate hydrophobicity stabilise either oil-in-water (O/W) or water-in-oil (W/O). Being of intermediate hydrophobicity, it could be imagined that systems incorporating these particles would be very sensitive to different conditions, and it is this idea which is followed up here. The energy with which a small spherical particle of radius r is held at an oil–water interface of interfacial tension $\gamma_{ow}$ is given by

$$E = \pi r^2 \sigma ow(1 \pm \theta)^2 \tag{2.1}$$

where $\theta$ in the contact angle between the disperse phase (water) with the continuous phase (oil) and the sign in the bracket is negative for $\theta < 90°$ and positive for $\theta > 90°$. We see from this that the values of both $\gamma ow$ and $\theta$ are important in determining the magnitude of the energy with which particles are anchored to interfaces, which in turn plays a role in establishing the effectiveness of particles in stabilising emulsions. The oil phases chosen range from non-polar hydrocarbons (of different structure) of relatively high $\gamma ow$ to polar alcohols or esters immiscible with water of relatively low $\gamma ow$. Likewise, water is replaced by a number of non-aqueous solvents.

Since the microfluidics utilizes the interaction between the interfacial tension and the fluidic shear force to break continuous fluids into uniform-sized segments, the effect of different viscosities of carrier oil on water-in-oil emulsion can be crucial, particularly how droplet size and droplet generation rate are affected.

As can be seen in Figure 2.6, the droplet size decreased as the oil viscosity increased. For instance, the average droplet size reduced from 43,6 to 39,5 (9,40% decrease), 35,5 (18,6% decrease), and 32,2 $\mu$m (26,1% decrease) to 7, 10, and 15 cSt at the flow pressure of 60:80 mbar (PW:PO), respectively. The declining trend of the droplet size displayed similar profiles over the increasing oil viscosity.

In addition, in the same figure, is also possible to analyse the effect of flow pressure levels, in other words, higher fluid flow of both solutions, on the droplet sizes. As the flow pressure became higher, the average droplet sizes for all different oil viscosity conditions dropped. This result is consistent with a previous studies where the volume of droplets decreased with an increase in the carrier fluid flow rate (i.e., the capillary number increased). The change was the most significant when the flow pressure changed from 30:40 to 60:80 mbar (PW:PO) with approximately 36%, 31%, 30%, and 30% decreases in average droplet size for 5, 7, 10, and 15 cSt, respectively.

In the Figure 2.7 is showed the effect of the oil viscosity on the droplet generation rate. Number of droplets generated per unit time decreased as more viscous oil was used under all tested flow pressure conditions, where strong linear correlations were observed ($R^2 > 0.96$ for all flow pressure conditions). For example, at a flow pressure level of 90:120 mbar (PW:PO), the droplet generation rate reduced from 239 to 215 (10% decrease), 182 (31% decrease), and 149 (38% decrease) droplets/min, when the oil viscosity changed from 5 to 7, 10, and 15 cSt, respectively ($R^2$ = 0.9949,. Similar trends were observed from all other flow pressure levels. This result indicates that the viscosity of the continuous phase is one

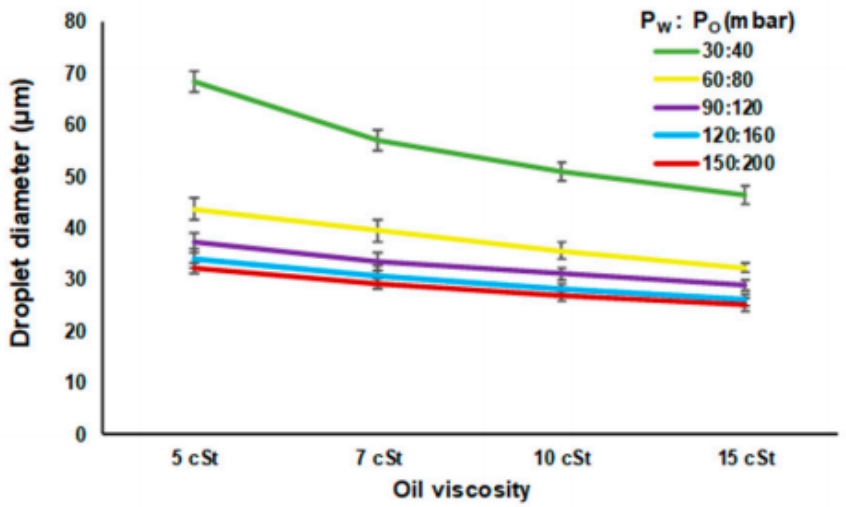


Figure 2.6: Water droplet diameter formed with different flow pressures and viscosities. [22]

of the dominant factors in the droplet generation, which affects the droplet generation rate independent of the flow pressures.

The droplet generation rate is also dependent on the flow rates of both oil and water solutions. As different flow pressure levels can change the flow rates of each solution. In this case, larger flow pressure levels, resulted in increase of the droplet generation rates, as showed in Figure 2.7. Fore example, when the flow pressure levels of water and oil changed from 30:40 mbar to 150:200 mbar for 5 cSt oil, the droplet generation rates increased from 76 droplets/min to 581. droplets/min

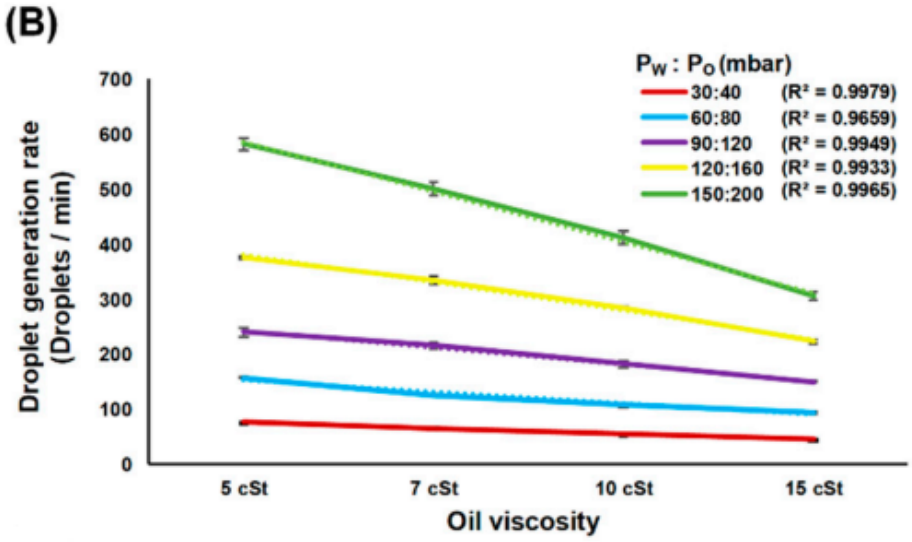


Figure 2.7: Droplate genaration rate for different pressures and viscosities. [22]

The figures showed that both the droplet size and the droplet generation rate decrease as higher viscosity carrier oil is used and as higher the flow rates of both phases.

### 2.5.1 Octamethyltrisiloxane

Octamethyltrisiloxane (OMTL) is a clear, colourless, viscous liquid. This component is effectively used as a solvent in electronic device cleaning systems [23]. It can be also used as a base of silicon oil. This form of the OMTL can be used for the production of microparticles using microfluidics devices.

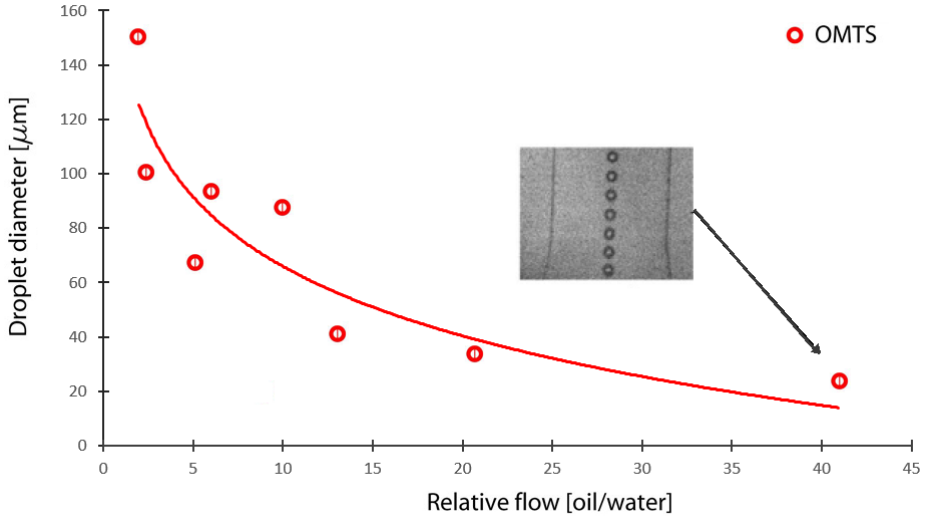


Figure 2.8: Diameter of monodisperse water-in-oil droplets for different flow ratios. [24]

The diameter of droplets (d) decreases with increasing flow ratio: $d=(Q_{oil}/Q_{water})^{-a}$ (a=0,57 for OTMS).

The size of droplets decreases exponentially with increasing flow rate ratios. Biggest tuning range and smallest droplet size is achieved with OMTS (Figure 2.8). The smallest droplets produced with OMTS are around 4 times smaller than the smallest droplets made with other oils like dioctyl phtalate or oleic acid, other oils used in microfluidics [24].

### 2.5.2 Alkanes

Another oil options that can be used in microfluidics as continuous phase are the alkanes. Alkanes are organic compounds, specifically hydrocarbon lipid molecules entirely consisted of hydrogen atoms and saturated carbon atoms that exist as liquid and are considered to be practically insoluble (in water) and relatively neutral [25]. They are oily liquids of the paraffin series used as a solvent, distillation chaser and scintillator components [26]. The next graphic shows the variation of the size of the droplets, relatively to the initial radius ($r_0$) as a function of time, for different alkanes.

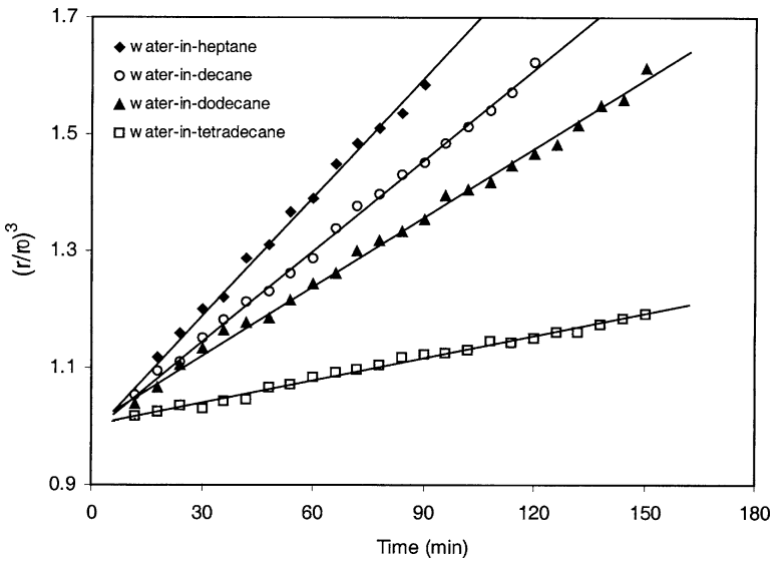


Figure 2.9: The normalized cube of the droplet size growth as a function of time in water-in-hydrocarbon emulsions.

[27]

As it is possible to see in the Figure 2.9, there is a significant variation of the size of the particles when a alkane with less carbons is used. In this way, it is preferable to use an alkane with a higher number of carbons. Another factor that influence in the preference between the alkanes is the stability in the liquid phase. Just alkanes with higher boiling point and lower melting point than the room temperature must be considered.

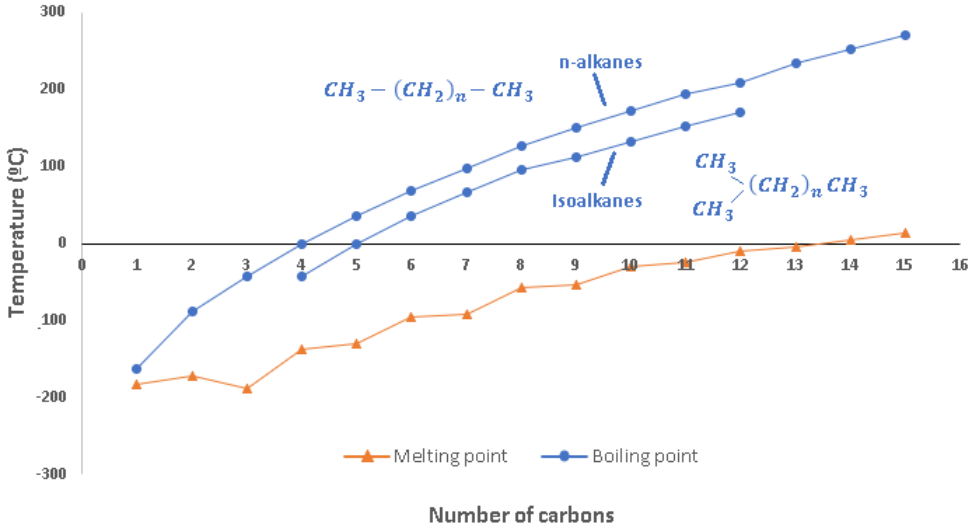


Figure 2.10: Melting (blue) of n-alkanes and boiling (orange) points of n-alkanes and isoalkanes in ℃.

.

The boiling points of the normal alkanes increase with increasing molecular weight Figure 2.10. As the molecular weight increases, London forces increase because more atoms are present to increase the surface area or the molecules. Simply put, there are more points of contact between neighboring molecules, and the London forces are stronger. The first four alkanes are gases at room temperature,

and solids do not begin to appear until about $C_{17}H_{36}$ , but this is imprecise because different isomers typically have different melting and boiling points. By the time you get 17 carbons into an alkane, there are a large numbers of isomers [28].

### 2.5.3 1-Undecanol

The presence of polar groups in the oil molecules play a decisive role in the emulsion stability, most probable via hydrogen-bonding interactions. Fatty alcohols and fatty acids are oils that due to their hydroxyl groups, they have a hydrogen bond (Figure 2.11).

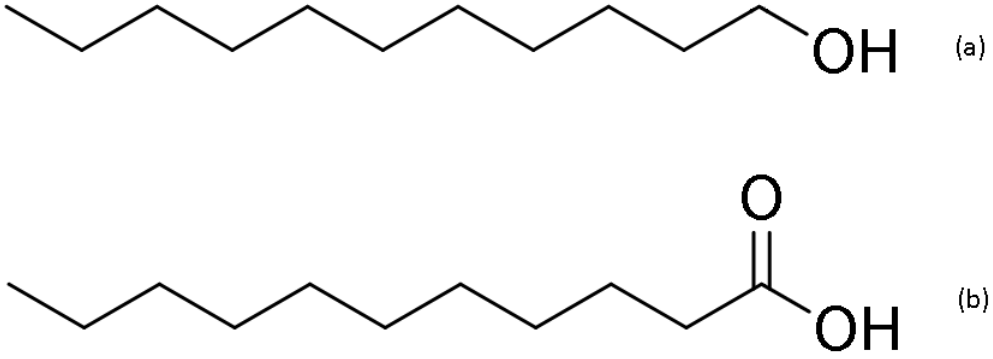


Figure 2.11: (a) Undecanol (fatty alcohol) (b) Undecylic acid (fatty acid)

.

However, the hydroxyl group of the fatty acid belongs to a carboxyl group, containing an additional double bounding oxygen. This causes a high polarity in the carboxyl group side of the molecule, provocating a significant interaction with water and causing micelles (Figure 2.12 of fatty acid around the molecules of water.

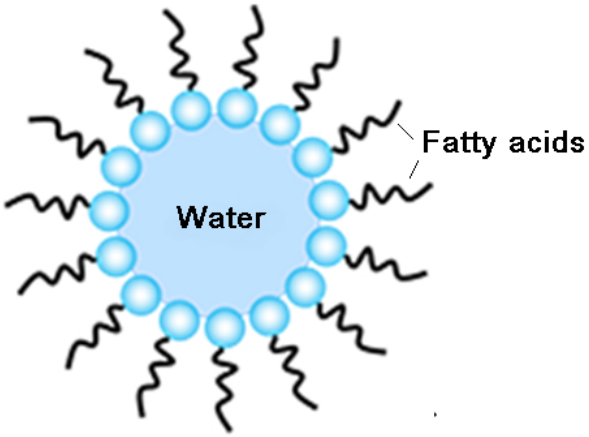


Figure 2.12: Schematic illustration of swollen micelles containing solubilized water.
[29]

Undecanol is a colorless fatty alcohol, insoluble in water and formed by 11 carbon atoms with simple covalent bound. Its 11 carbons allow undecanol to be in liquid form at room temperature, having a boiling temperature of 243 ºC. Furthermore, since it does not have so many carbons, there are limited isomers

of this molecule.

Undecanol–water interfacial tension is fairly low (9.5 mN $m^{-1}$) and the undecanol–water contact angle is reasonably high (160°). Both of these facts lead to the prediction that this emulsions would have low stability. However, despite the emulsion eventually destabilise completely into the parent liquid phases, immediately after preparation they can be gel-like of high viscosity. The timescale for this depends on the water flow rate and, surprisingly, critically on temperature. At fixed flow rate, the emulsion stability passes through a sharp maximum with respect to temperature [30].

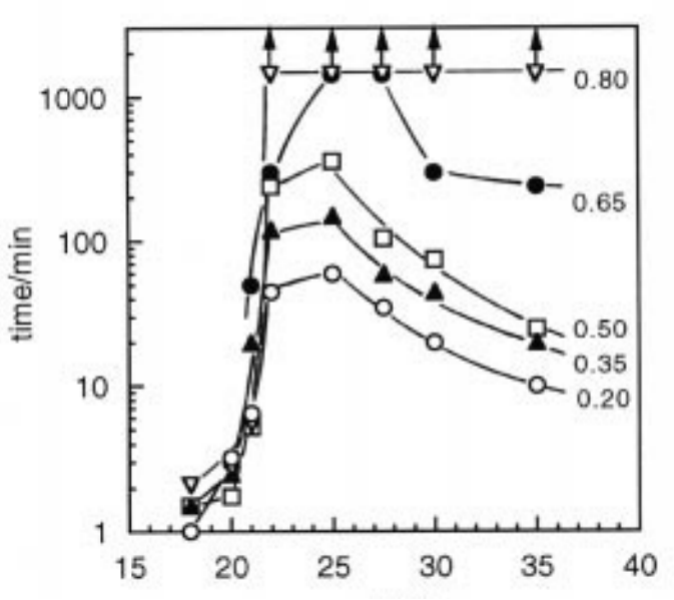


Figure 2.13: Stability of water-in-undecanol emulsions stabilised as a function of temperature and volume fraction of water.

[30]

For different fractions of water in the emulsion, it's possible to observe a higher stability time for a temperature of 25ºC (Figure 2.13). Thus, undecanol is a highly recommended oil for microfluids at room temperature, leading to the formation of stable particles when used with aqueous solutions.

# Chapter 3

# Drug delivery particles

## 3.1 Alginate for microfluidics

Various microfluidic approaches have been developed for generating hydrogel microparticles. Among them, alginate hydrogels have been particularly attractive in wound healing, drug delivery, and tissue engineering applications.

Alginate is a natural polysaccharide composed by blocks of copolymers with different ratio of guluronate to mannuronate depending on the natural source. Despite being biocompatible, alginate promotes very low protein adsorption due to its high hydrophilicity, being therefore considered a non-fouling material. Alginate is now known to be a whole family of linear copolymers containing blocks of (1,4)-linked $\beta$-D-mannuronate (M) and $\alpha$-L-guluronate (G) residues. The blocks are composed of consecutive G residues (GGGGGG), consecutive M residues (MMMMMM), and alternating M and G residues (GMGMGM) (Figure 3.1) [31]. Gels prepared from alginate with a high content of G residues exhibit higher stiffness than those with a low amount of G residues. Their blocks differs in both the distribution as well as the length regarding species in addition the extracted portion of the alginate from seaweed. Also, as a result of the naturally occurring polysaccharide, alginate exhibits a pH-dependent anionic nature and has the ability to interact with cationic polyelectrolytes and proteoglycans. Therefore, delivery systems for cationic drugs and molecules can be obtained through simple electrostatic interactions. Due to its outstanding properties in terms of biocompatibility, biodegradability, non-antigenicity and chelating ability, alginate has been widely used in a variety of biomedical applications including tissue engineering, drug delivery and in some formulations preventing gastric reflux[32].

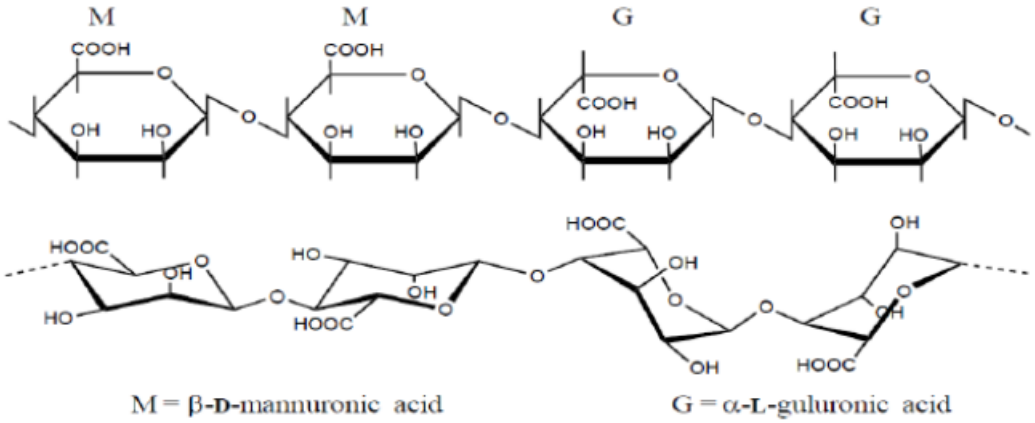


Figure 3.1: Structure of alginate shown as the alternating segment of ..MMGG.. residues. [33]

Hydrogels are three-dimensionally cross-linked networks, which are composed of hydrophilic polymers with high water content Alginate hydrogels are three-dimensionally cross-linked networks composed of hydrophilic polymers with high water content. These gels retain structural similarity to the extracellular matrices in tissues and can be manipulated to play several critical roles.

The hydrogel droplet formation can be classified in two types, depending if alginate particles are gelated by either external gelation or internal gelation. Internal gelation of alginate droplets generally utilizes poorly soluble salts of divalent cations. This internal gelation process provides control over the time period of reaction and can maintain the spherical structure of alginate particles but produce partially and incomplete cross-linked particles with weak stiffness as the gelation progress is dependent on the diffusion of ions from the inner core to the particle surface. External gelation of alginate droplets occurs when the divalent cations necessary for the reaction are in the CaCl2 solution droplets, off-chip bulk solution, or supplied directly through the oil phase. This method often leads to clogging issues and non-uniform hydrogel formation due to the high reaction speed and heterogeneous distribution of divalent cations inside devices [34].

Chemical and/or physical cross-linking of hydrophilic polymers are typical approaches to form alginate hydrogels , and their physicochemical properties are highly dependent on the cross-linking type and cross-linking density, in addition to the molecular weight and chemical composition of the polymers. Many methods have been employed for preparation of alginate hydrogels, including ionic interaction, covalente interaction, phase transition (thermal gelation), cell-cross-linking, free radical polymerization and “click” reaction [32]

### 3.1.1 Ionic interaction

The most common method to prepare hydrogels from an aqueous alginate solution is to combine the solution with ionic cross-linking agents, such as divalent cations. The divalent cations are believed to bind solely to guluronate blocks of the alginate chains, as the structure of the guluronate blocks allows a high degree of coordination of the divalent ions. The guluronate blocks of one polymer then form junctions with the guluronate blocks of adjacent polymer chains in what is termed the egg-box model of cross-linking, resulting in a gel structure.

The gelation rate is a critical factor in controlling gel uniformity and strength when using divalent cations, a slower gelation produces more uniform structures and greater mechanical integrity. The gelation rate depends on the temperature. At lower temperatures, the reactivity of ionic cross-linkers is

reduced, and cross-linking becomes slower. The resulting cross-linked network structure has greater order, leading to enhanced mechanical properties. In addition, the mechanical properties of ionically cross-linked alginate gels can vary significantly depending on the chemical structure of alginate[31].

Over the past decade, ionic cross-linked alginate hydrogels have been developed and employed in a variety of settings, such as alginate cross-linked with $Ca^{2+}$, $Mg^{2+}$, $Fe^{2+}$, $Ba^{2+}$, or $Sr^{2+}$. Usually, the $Ca^{2+}$ (Figure 3.2) is the most commonly used divalent cations [32].

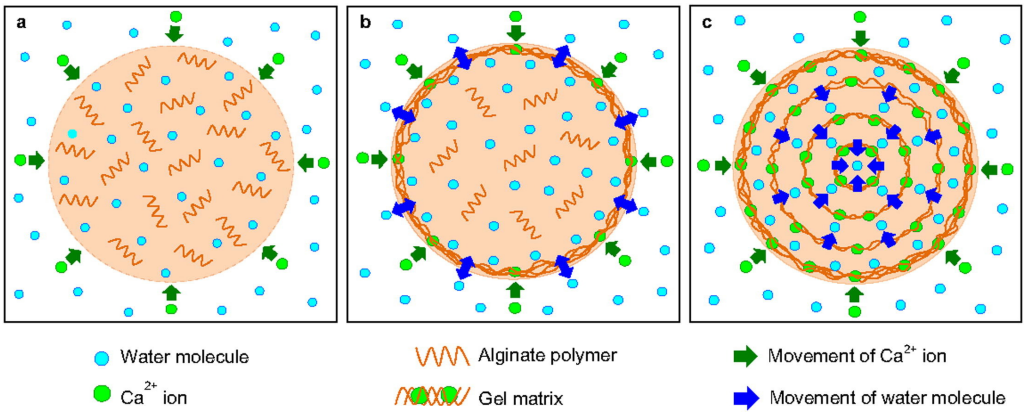


Figure 3.2: External gelation of alginate.
[35]

$CaCl_2$ is the most commonly exploited ionic cross-linking agent. Owing to the high solubility of $CaCl_2$ in the aqueous medium, the alginate gelation rate is too high to control. In order to retarded gelation speed, $CaSO_4$ and $CaCO_3$ could be used instead. Their poor solubility in aqueous solution increases the aging time of the alginate. Also, a phosphate-containing buffer (e.g., sodium hexametaphosphate) could be used since phosphate groups in the buffer competed with the carboxylate groups of the alginates in the reaction with calcium ions, and lowering the gelation [36].

### 3.1.2 Covalent transition

Covalent cross-linking is the process of linking polymer chains by covalent bondings, forming tridimensional networks which reduce the mobility of the structure and usually enhance its mechanical and barrier properties [37]. Covalent cross-linking improves chemical and mechanical properties of the material and has been used for many different materials and applications [38]. Covalent cross-linking covered here involves utilizing a cross-linking agent to junk two polymer chains. The cross-linking of the natural and synthetic polymers could be achieved through the reaction of their functional groups (including -OH, -COOH, and -NH2) with cross-linkers such as glutaraldehyde, adipic acid dihydrazide, poly (ethylene glycol)-diamine. [36].

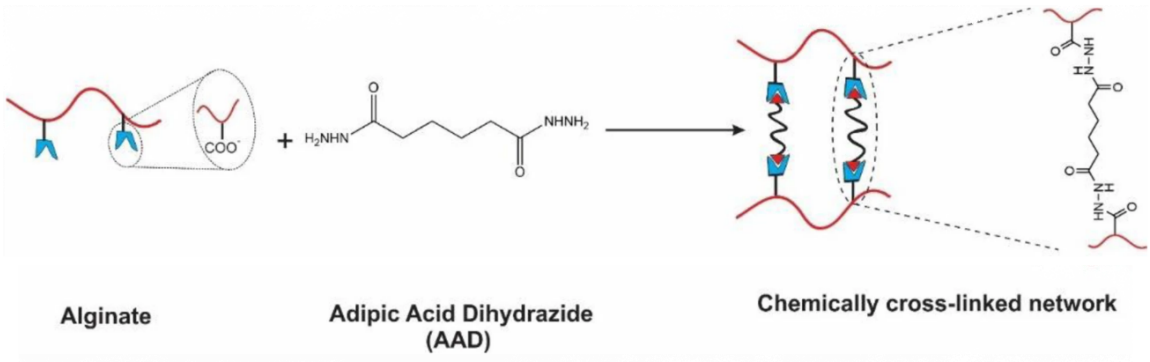


Figure 3.3: Schematic showing of covalent cross-linking of alginate using adipic acid dihydrazide as cross-linker.

[39]

As depicted in Figure 3.3, the alginate gels with covalent cross-linking are normally generated by the reaction between carboxylic groups in two different alginate branches and a cross-linking molecule possessing primary diamines. cross-linking density directly influences on the mechanical properties of the hydrogels; however, swelling property is significantly controlled by the type of the cross-linking molecules. Utilizing hydrophilic molecules as a second macromolecule (e.g., polyethylene glycol) compensates for the reduction of the hydrophilic character during the cross-linking process.

### 3.1.3 Phase transition

The phase transition phenomenon in which a material goes from a solution to a gel state is usually referred to as a sol-gel phase transition. Some hydrogels become solidified like a gel and make a separate layer from the solution above a certain temperature (Figure 3.4. This temperature threshold limit is well defined as the lower critical solution temperature (LCST)[40].

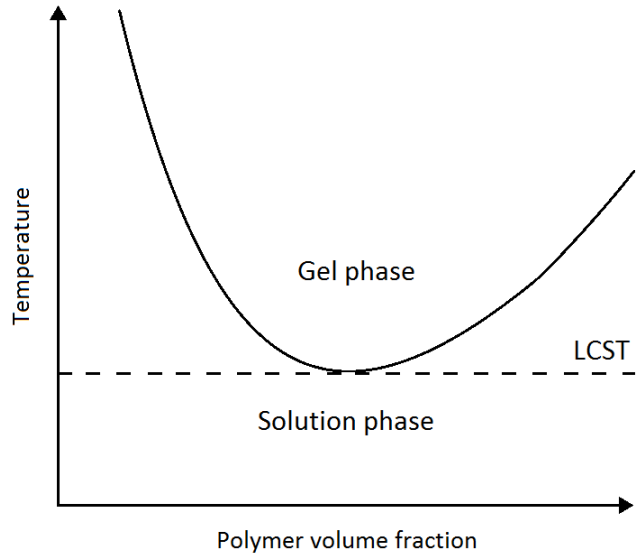


Figure 3.4: Schematic diagram of the relationship between temperature and hydrogel structural behavior with reference to the lower critical solution temperature

The most remarkable property of thermoresponsive gels is that, they do not require a chemical

stimulus in order to undergo phase transition. There are multiple mechanisms and theories describing thermo-gelation or phase transition in the aqueous solutions. The main mechanism is a change in the hydration state that favors intra and intermolecular hydrogen bonding, which ultimately decreases or increases the solubility of hydrogels upon temperature change[40]. Poly(N-isopropylacrylamide) (PNIPAAm) is well known for its ability to show LCST behavior in aqueous solutions at 32 ℃. The thermosensitivity of an alginate hydrogel can be achieved by incorporating PNIPAAm into its backbone. Figure 3.5 shows a schematic representing the temperature dependent behavior of PNIPAAm grafted alginate (PNIPAAm-g-Alginate) hydrogels.

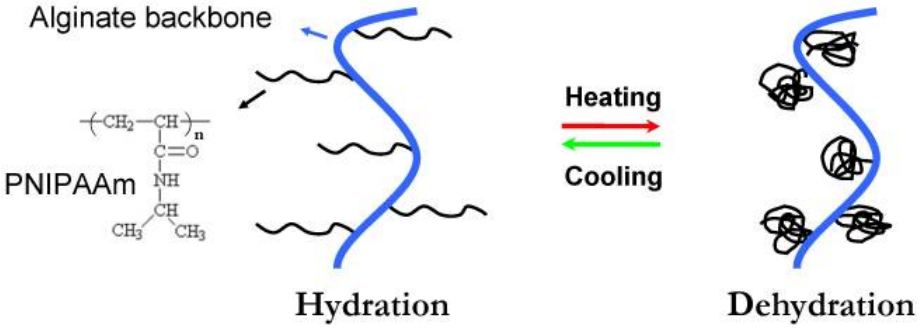


Figure 3.5: Schematic representation showing the temperature dependent behavior of PNIPAAm-g-alginate hydrogels. PNIPAAm = Poly(N-isopropylacrylamide).
[32]

Many reports have shown that thermoreversible alginate hydrogels that reversibly form a gel in response to the simultaneous variation of at least two physical parameters (e.g., pH, temperature, or ionic strength) can be blended to target their physical and mechanical properties [32].

### 3.1.4 Cell cross-linking

Specific receptor-ligand interactions have been employed to cross-link alginate hydrogels. Although it exhibits good biocompatibility, alginate is composed of inert monomers that inherently lack the bioactive ligands necessary for cell anchoring. The strategy of cell-cross-linking is to introduce ligands, e.g., arginine-glycine-aspartic acid (Arg-Gly-Asp, RGD) sequence onto alginate for cell adhesion by chemically coupling utilizing water-soluble carbodiimide chemistry. Once mammalian cells have been added to this RGD-modified alginate to form a uniform dispersion within the solution, the receptors on the cell surface can bind to ligands of the modified alginate. The RGD-modified alginate solution has been subsequently cross-linked to form network structures via specific receptor-ligand interactions between cell surface and RGD sequences (Figure 3.6). Although the cell cross-linked hydrogel shows excellent bioactivities, the network exhibits low strength and toughness, which may limit its practical applications.

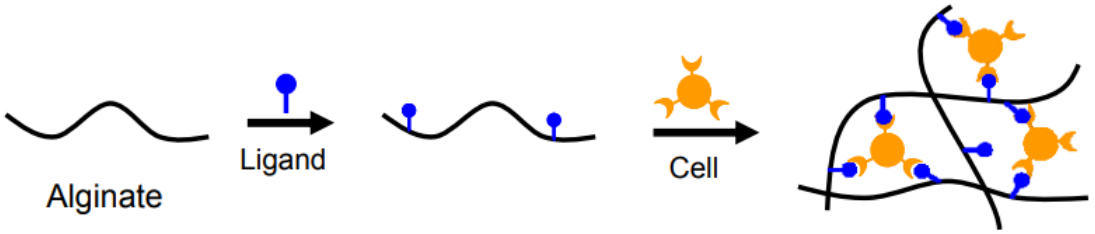


Figure 3.6: Schematic representation showing cell cross-linked network formation of ligand modified alginate.

[32]

### 3.1.5 Free radical polymerization

Free radical polymerization means the process of transforming linear polymer into a three-dimensional polymer network, which can be carried out at physiological pH and temperature with the appropriate chemical initiators (Figure 3.7), even in direct contact with drugs and cells [32]. Many of these addition reactions are known to proceed in a stepwise fashion by way of reactive intermediates, and this is the mechanism followed by most polymerizations.

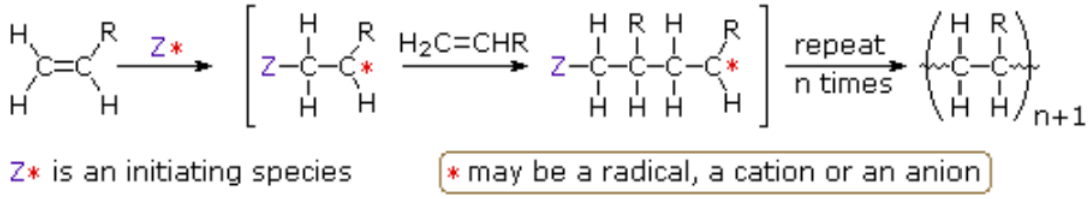


Figure 3.7: Schematic representation of polymerization using a radical, a cation or an anion.

[41]

It is useful to distinguish four polymerization procedures fitting this general description.

- Radical polymerization: the initiator is a radical, and the propagating site of reactivity is a carbon radical;
- Cationic polymerization: the initiator is an acid, and the propagating site of reactivity is a carbocation;
- Anionic polymerization: the initiator is a nucleophile, and the propagating site of reactivity is a carboanion;
- Coordination catalytic polymerization: the initiator is a transition metal complex, and the propagating site of reactivity is a terminal catalytic complex [41].

This can provide better temporal and spatial control over the gelation process. The unique advantage of chain polymerization is the ease with which a variety of chemistries can be incorporated into the hydrogel by simply mixing derivatized macromers of choice and subsequently copolymerizing.

Many researchers have been interested in exploiting free radical polymerization of methacrylated alginate with unsaturated C=C double bond groups to create hydrogels as cell delivery vehicles for tissue regeneration (Figure 3.8). An extensively studied methacrylated alginate hydrogel is formed by employing ultraviolet (UV) irradiation to generate radicals from appropriate photoinitiators, which further react with the active end group on the methacrylated alginate to form covalent cross-linked bonds [32].

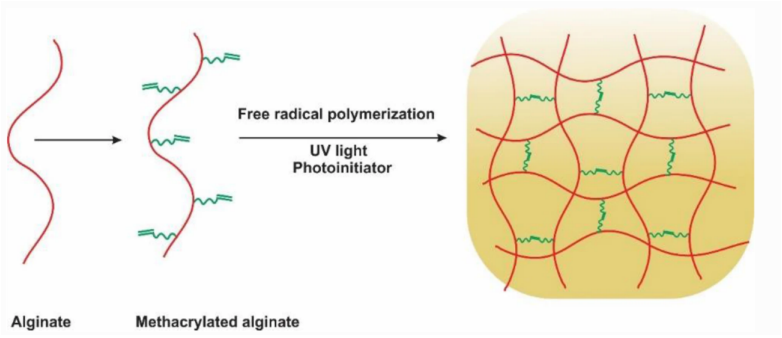


Figure 3.8: Preparation of methacrylated alginate and photocross-linking of methacrylated alginate. [39]

### 3.1.6 Click reaction

Click chemistry refers to a group of reactions that are fast, simple to use, easy to purify, versatile, regiospecific, and give high product yields [42]. This operation describes an adjusted chemical operation to generate substances quickly and reliably by bonding small units together. The most common example being 1,3-dipolar cyclo additions, the copper (I)-catalyzed reaction of azides with alkynes. While the versatility of metal-mediated "click" reactions has been broadly exploited, a major limitation is the intrinsic toxicity of transition metals and the inability to translate these approaches. The Schiff-base reaction (Figure 3.9) between aldehyde groups of oxidized alginate and amino groups of gelatin had been seen as a viable way of producing alginate-gelatin composite hydrogel .

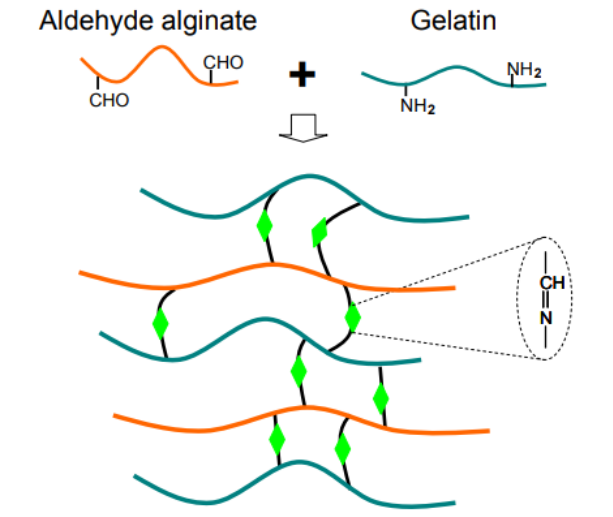


Figure 3.9: Alginate-gelatin composite hydrogel via the Schiff-base reaction. [32]

Nowadays the major issue is to design bioactive alginate-based hydrogels that would be readily injectable at or below room temperature, would form gels with relatively appropriate biodegradable properties under physiological conditions, and would support cell induction. There is a continuing need to exploit novel cross-linking methods to enhance bioactive and mechanical properties of alginate hydrogels [32].

## 3.2 Drug delivery

Appropriate local targeting is a challenge in the treatment of cancer. For improved localization, a well designed drug delivery system is beneficial to enhance therapeutic efficacy. There are many approaches used for appropriate targeting like pro drug approach, conjugate approach, and time released system, pH dependent system, multiparticulate system, nanoparticulate system, probiotic approach. Among all, microparticles system have turned out to be a promising approach as a targeted drug delivery system for the treatment of this disease. The main aim for the targeted drug strategy is to target the right amount, at right time of active agents in inflamed intestinal tissues by using selective delivery to achieve therapeutic efficacy while simultaneously reducing adverse effects. In addition to this, such targeted delivery system must meet the conditions for complete biodegradation and high biocompatibility without pro-inflammatory properties.

This microparticles consists in small free flowing particles consisting of natural or synthetic polymers having particle diameter ranging from 1 to 1000 $\mu$m [43]. Controlled release drug delivery system is one of the most efficient methods to overcome most of the difficulties associated with other methods of administration. However, due to various problems such as low solubility, poor stability, narrow therapeutic index of many new drugs, there is a corresponding need for safer drug delivery. Controlled release drug delivery includes carriers such as polymer-based disks, microparticles, nanoparticles, pellets in which drug gets encapsulated and release at controlled rates for relatively long periods of time. Such kind of systems often show several advantages over other methods of administration.

- First advantage is the drug release rates can be adjusted according to the needs of a specific application; for example, providing a constant rate of delivery or pulsatile release
- Second, controlled release systems also protect drugs, especially proteins, from degradation that are otherwise rapidly destroyed by the body. Finally, by using controlled release systems, frequent (daily) dosing can be replaced by giving once per month injection, which ultimately increases patient comfort and compliance.

### 3.2.1 Types and mechanism of drug release

The process of drug release of microparticles, produced by special manufacturing technologies and/or possibly containing special excipient(s), is the result of various phenomena and mechanisms (dissolution/diffusion, osmotically driven release, erosion) (Figure 3.10). Generally, these mechanisms take place side by side and one or the other mechanism provides a greater role during drug release. In the microparticles, when the active pharmaceutical ingredient is embedded in a polymer matrix , the behavior of the polymer system is crucial during dissolution, but depends on many factors (drug properties, formulation, release medium, etc.).

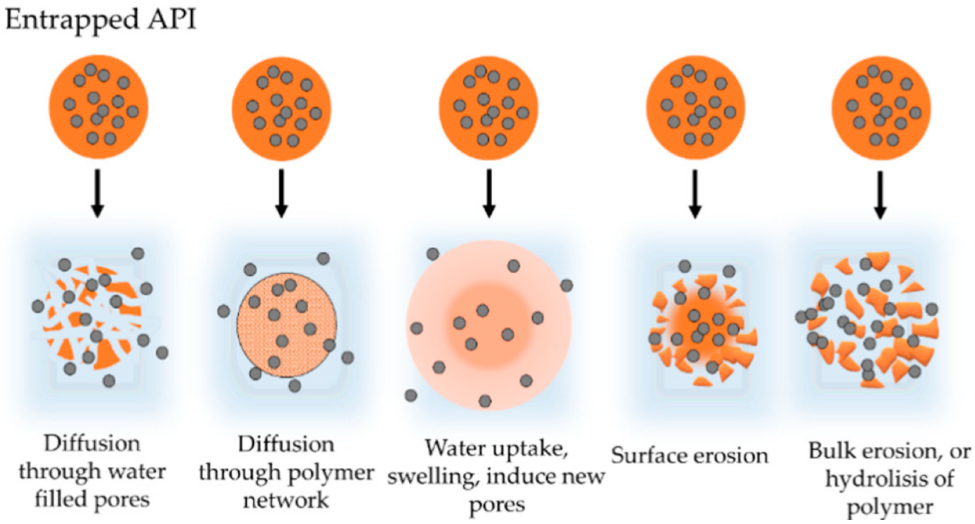


Figure 3.10: Release mechanisms in microencapsulated products.
[44]

In the case of a polymer matrix, the diffusion of the active ingredient can be through the intact polymer network or through the pores filled with water. Water-soluble drugs may also dissolve in the aqueous pore networks. Water uptake causes polymer chains to swell, indicating the formation of new pores and/or osmotic pressure. During swelling, the volume increases, the effective diffusion coefficient of the drug is increased, and more pharmacon molecules enter the aqueous part. Erosion of the polymer matrix (bulk/surface) is also possible [44].

### 3.2.2 Reservoir

If the drug and the release rate controlling material (often a polymer) are separated according to a core–shell structure, the drug being located in the center and the release rate controlling material forming a membrane surrounding this drug depot, then the device is called a “reservoir system.” In this case, the polymer reservoir may dissolve in the medium or act as a water-insoluble, permeable or semipermeable membrane. In the former case, the diffusion is predominantly due to the release of the active ingredient. In the case of a semipermeable coating, the osmotic phenomenon should be taken into account. It is also possible to use water-soluble pore formers, which, by creating pores, accelerate the dissolution profile (Figure 3.11).

Reservoir systems can be further classified as having either a nonconstant activity source” or a “constant activity source.” In the first case, drug concentration in the reservoir is below its solubility. Thus, drug molecules that are released across the membrane are not replaced, and the drug concentration at the inner membrane’s surface decreases with time. In reservoir systems with a constant activity source, an excess of drug is provided in the depot and released drug molecules are rapidly replaced by dissolution of the remaining nondissolved drug excess. Consequently, the drug concentration at the inner membrane’s surface remains constant as long as drug is present in excess. When the reservoir’s drug concentration falls below solubility, the reservoir becomes a nonconstant activity source. Note that the relevant solubility is that of the drug in the wetted depot at body temperature, not the drug’s solubility in the pure release medium or the drug solubility in the dry depot. In practice, it is often difficult to know the exact drug solubility in the system’s core upon water penetration at 37℃ and caution should be paid, since dissolution of other core compounds (e.g., sucrose and acid) might significantly affect the solubility of the drug

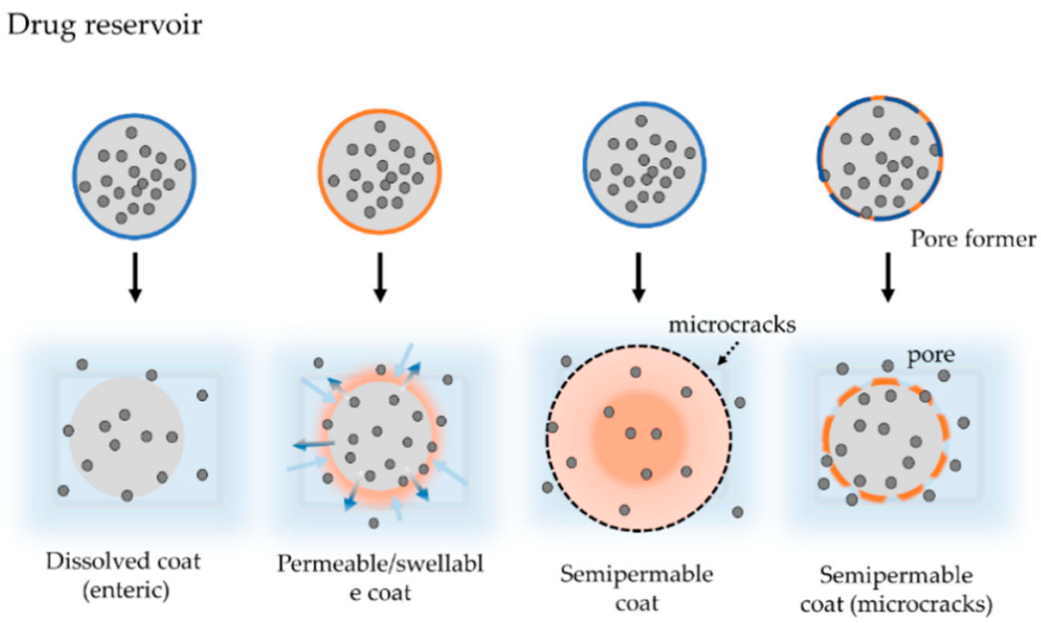


Figure 3.11: Reservoir micro encapsulation release.
[44]

### 3.2.3 Diffusion mechanism

Diffusion plays a major role in most controlled drug delivery systems. Diffusional mass transport is of fundamental importance for numerous processes in the body and nature in general. The basic idea is that a solute diffuses from regions of higher concentration to adjacent regions of lower concentration. Considering diffusion in a single direction, x, Fick's First Law (FFL) relates diffusion flux, J (mass flow per unit area) to the gradient in solute concentration, c, according to

$$J = -D_{\mathrm{f}} \frac{\delta c}{\delta x} \tag{3.1}$$

where D is the diffusion coefficient, or diffusivity. Assuming that the solute is neither created nor consumed during the process, the local change in concentration with time in a thin sliver of solution between points x and x + dx is determined by mass balance according to the difference in flux into the sliver at x and out at x + dx. As this sliver becomes infinitely small, this mass balance can be written as

$$\frac{\delta c}{\delta t} = -\frac{\delta J}{\delta x} \tag{3.2}$$

Combining (Equation 3.1) and (Equation 3.2) we arrive at Fick's second law, also known as the diffusion equation

$$\frac{\delta c}{\delta t} = \frac{\delta}{\delta x} D(\frac{\delta c}{\delta x}) \tag{3.3}$$

Considering all three spatial dimensions, x, y, and z, and allowing the diffusion coefficient to vary with position, time, and/or solute concentration (3.3) generalizes to:

$$\frac{\delta c}{\delta t} = \frac{\delta}{\delta x} D(\frac{\delta c}{\delta x}) + \frac{\delta}{\delta y} D(\frac{\delta c}{\delta y}) + \frac{\delta}{\delta z} D(\frac{\delta c}{\delta z}) \tag{3.4}$$

The diffusion equation can be solved when initial and boundary conditions are specified. However, for delivery systems with time, position and/or concentration dependent diffusion coefficients, generally no analytical solution of Fick's law is available. The same is true for devices with complex shapes. In

these cases, numerical techniques can be used to calculate mass transport.

Often, the overall release rate is affected by several physical and chemical phenomena. Obviously, diffusion is the mass transport mechanism when other processes are not involved in the control of drug release. Alternatively, diffusion is dominant if the impact of all other phenomena is negligible. If several processes take place in series and one of these steps is much slower than all the others, this slowest process is dominant. For the quantitative description of the overall release rate, only the slowest step needs to be taken into account. Also, if a matrix forming material starts to degrade only after complete drug exhaust, then degradation is not involved in the control of drug release, and there is no need to consider it in a mathematical model quantifying drug release [45].

### 3.2.4 Diffusion coefficient

The diffusion coefficient of drug in the matrix material is a measure of the mobility of drug in the material. The importance of diffusion coefficients in mass transfer operations have been well recognized. Howeve, an exact theoretical equation for the evaluation of diffusion coefficients is still not available since the kinetic theory of liquids is incompletely developed.

A wide variety of correlations are available for this purpose. For the diffusion in dilute solutions, the correlations of Wilke and Chang seems to be useful. It is the proportionality between flux and concentration gradient. The method of Wilke and Chang (3.5) represents the widely accepted standard for prediction of diffusion coefficients:

$$D = \frac{7{,}4 \times 10^{-8} (\phi_{\mathrm{s}} M_{\mathrm{s}})^{1/2} T}{\eta_{\mathrm{s}} {V_{\mathrm{D}}}^{0{,}6}} \tag{3.5}$$

Where $M_s$ is the molecular weight of the solvent, T is the temperature, $\eta_s$ is the solvent viscosity and $V_D$ is the molar volume of solute at boiling point. Like every correlation, it has its own drawbacks. This correlates most of the experimental values within an average deviation of ± 13%. But the trouble comes when one must find the association parameter ($\phi_{\mathrm{s}}$) for unknown systems. The association parameter was introduced in the above equation to define the effective molecular weight of the solvent with respect to the diffusion process. Apart from the difficulty of getting this parameter for an unknown system, the value of 1.0 for organic unassociated solvents and 2.6 for water may probably lead to errors in the diffusion values as pointed out by Garner and Merchant. According to them, for alcohols with a big chain of carbon atoms diffusing into water, such as undecanol, the parameter of 2.6 is approximately correct [46].

## 3.3 COMSOL Multiphysics Software

Following with the major boost brought by computer technology, more and more computer software has been widely developed and used in the arena of engineering. The usage of the software can help engineers to solve problems efficiently. COMSOL Multiphysics is a finite element analysis, solver and Simulation software package for solving various physics and engineering applications. The first version of COMSOL Multiphysics software was published in 1998 by COMSOL group and it was named as Toolbox. At the beginning time, this software is only applied in the field of Structural Mechanics. The COMSOL Multiphysics simulation environment facilitates all steps in the modeling process defining your geometry, specifying your physics, meshing, solving and then post-processing your results [47].

There are several application-specific modules in COMSOL Multiphysics. The most common applications are

- AC/DC Module
- Acoustics Module
- CAD Import Module
- Chemical Engineering Module
- Earth Science Module
- Heat Transfer Module
- Material Library

The spread usage of COMSOL Multiphysics in various domains largely depends on its marked characteristics, such as solving multi-physics problem, specifying own Partial Differential Equations or e.xuberance of simulation capability [48].

# Chapter 4

# Experimental part

## 4.1 Material

A description of the compounds used and some of their properties are described in Table 4.1 and Table 4.2.

Table 4.1: Compounds used and their suppliers.

| Classification | Compound | CAS | Manufacture |
|---|---|---|---|
| *Amino acids* | Glycine | 56-40-6 | Penta |
| *Aldehyde* | Glutaraldehyde | 111-30-8 | Sigma-Aldrich |
| *Buffer* | Phosphate-buffered saline | 9003-39-8 | Sigm-Aldrich |
| *Oil* | 1-undecanol | 112-42-5 | Sigma-Aldrich |
| *Polymer* | Polydimethylsiloxane | 9016-00-6 | DOW |
| | Norland Optical Adhesive | 1025-15-6 | Norland |
| *Polysaccharide* | Chitosan | 9012-76-4 | Sigma-Aldrich |
| | Alginate | 9005-32-7 | FMC Biopolymer |
| *Salts* | Iron(II) chloride tetrahydrate | 13478-10-9 | Sigma-Aldrich |
| | Iron(III) chloride hexahydrate | 10025-77-1 | Sigma-Aldrich |
| | Trisodium citrate dihydrate | 6132-04-3 | Sigma-Aldrich |
| | Calcium iodide | 10102-68-8 | Sigma-Aldrich |
| *Solvent* | Ammonium hydroxide | 1336-21-6 | Sigma-Aldrich |
| | Deionized water | 7732-18-5 | Aqual 25 |
| | Acetic acid | 64-19-7 | Penta |
| *Surfactant* | ABIL | 6683-19-8 | Prospector |

Table 4.2: Physical and chemical properties of the compounds employed.

| | **Grade** | **$\rho$ (g/cm$^3$)**[a] | **Viscosity (mPa.s)**[a] | **B.P. (°C)** |
|---|---|---|---|---|
| 1-undecanol | 99% | 0,83 | 21,20 | 243,0 |
| Acetic acid | 99% | 1,05 | 1,140 | 117,9 |
| Ammonium hydroxide | 30% | 0,88 | 1,770 | 37,70 |
| Calcium iodide | 99% | 3,96 | - | 1100 |
| Chitosan | <=100% | 0,23 | - | - |
| Deionized water | - | 1,00 | 0,889 | 100,0 |
| Glutaraldehyde | 50% | 1,06 | 13,06 | 187,0 |
| Glycine | 99% | 1,16 | 46,30 | 146,3 |
| Iron(II) chloride tetrahydrate | >99% | 1,93 | - | 1026 |
| Iron(III) chloride tetrahydrate | 97% | 1,82 | - | 283,1 |
| Norland Optical Adhesive[b] | <=100% | >1,00 | 300,0 | - |
| Polydimethisiloxane[b] | <=100% | 1,03 | 3500 | 200,3 |
| Trisodium citrate dihydrate | 99% | 0,60 | - | - |

[a] at 25°C

[b] values of viscosity before polymerization

## 4.2 Methods

### 4.2.1 Chip production

There are two processes for producing PDMS microchips, each with its own advantages and disadvantages.Using plasma surface activation for bonding the microchips parts or heating attachment, coming in contact the surfaces when they are not completely solid and taking advantage of the curing process. The first process allows a great bonding of the microchip parts. However, the hydrophilic character of the microchip after plasma treatment can be a problem. On the other hand, heat attachment allows to produce microchips in a short time but can produce air bubbles inside the microchip.

The PDMS microchips were fabricated by pouring a degassed mixture of Sylgard 184 silicone elastomer and curing agent onto master microchip mold on silicon wafer with positive relief for microchip top as well as a blank Petri dish for bottom. For each process different base/curing agent ratio were used (Table 4.3).

Table 4.3: Ratio of the mixture between elastomer base and curing agent for heat attachment and surface activation process.

| | **Ratio base/curing agent** | |
|---|---|---|
| | Upper | Bottom |
| **Surface activation** | 10:1 | 10:1 |
| **Heat attachment** | 5:1 | 14:1 |

After degassed in a desiccator, the wafer and Petri dish with polymer was cured in an oven, at 70°C, for 2 hours for surface activation and around 20 min for heat attachment, until the microchip parts achieve enough hardness to preserve the pattern.

#### 4.2.1.1 Pattern clearing

The PDMS microchip was cut with a curved razor blade, gently lifting the excised pieces from the master mold, inserting microwires into designated inlets and outlet channels and traces of dust were removed from the both parts of the microchip by scotch tape.

#### 4.2.1.2 Parts assembly

The last part of the microchip production is assembling the parts. As mentioned before, plasma can be used for this. Plasma, as the fourth state of matter, is generated by heating or subjecting a neutral gas to electromagnetic fields. It is composed of a high concentration of reactive species, including ions, electrons, neutrons, excited molecules, free radicals, metastable particles and photons that are capable of inducing physical and chemical changes on polymeric surfaces (Figure 4.1). When an object undergoes a plasma bonding process, the surface energy is raised due to bombardment of charged particles of the plasma such as ionized atoms or molecules and electrons that react chemically with the surface by sputtering effect.

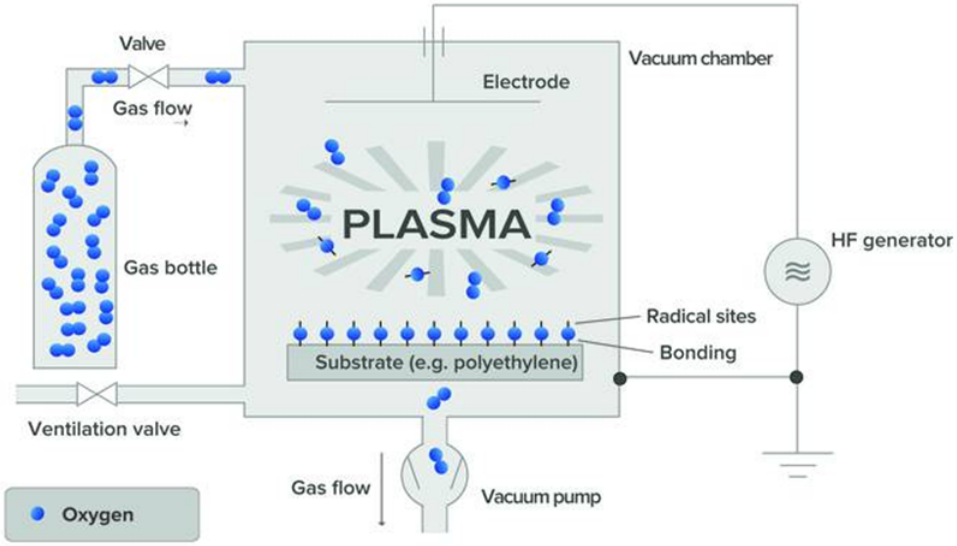


Figure 4.1: Schematic representation showing Surface activation using oxygen plasma . [49]

It was used Diener Zepto plasma system for the surface activation and defining the following parameters, the top part was sticked to the bottom part:

- Pressure - stable between 0,2 and 0,3 mbar;
- Power - 30%;

After 50 seconds under plasma surface activation the microchip was assembled and left 48 hours into the oven at 70℃ for removing the hydrophilicity caused by the plasma.

For the preparation of these chips with heat attachment, the two parts of the chip are bonded when the surfaces are not completely solid so they can attach easily without using the plasma surface activation. After pattern clearing, the parts were assembled and left into the oven at 70℃ for over 2h (Figure 4.2).

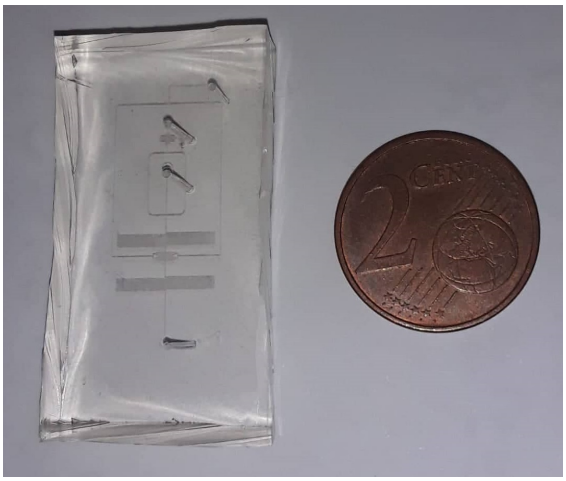

Figure 4.2: Device prepared from PDMS and the comparison of its size with a coin (the length of the whole device is around 4 cm)

### 4.2.2 Replication of silicon wafer master mold

In order to turn the production of microchips more efficient, master mold was replicated since some units from this mold were damaged so were useless. In this way, more chips could be produced with the same amount of PDMS. The replication was done in a glass Petri dish, using NOA (Norland Optical Adhesive) for producing a positive relieve on it. NOA is a liquid adhesive component that cures in seconds to a tough, hard polymer when exposed to ultraviolet light. It can provide excellent light transmission over a wide spectral range.

#### 4.2.2.1 Preparation of microchips

Initially, upper part units of a PDMS microchip were done with a ratio 10:1 and following the same process described in the section 4.2.1.1. After cutting the microchips with a curved razor blade, was no needed to make the inlets and outlet channels.

#### 4.2.2.2 UV curing

Two drops NOA were spilled on a glass Petri dish for each microchip that would be replicated. The microchips prepared before were set down on the drops. After degassification, the NOA was cured under UV light for 10 minutes. The microchips were unsticked from the NOA carefully in order to leave a positive-relief on the glass Petri dish.

### 4.2.3 Preparation of dispersed phase solution

#### 4.2.3.1 Preparation of iron oxide nanoparticles

For preparation of the solution of iron oxide, iron(III) chloride hexahydrate and iron(II) chloride tetrahydrate are diluted in water in the proportion 3:1,5:100 (w/w) and stirred for 10 min at 475 rpm. After slowly increasing of the temperature to 80℃ during 10 minutes, it was added 20 ml of ammonium hidroxide and 10 ml after 1 hour. The solution continue stirring for 1h and then an 48 ml of aqueous solution of trisodium citrate dihydrate, 5:1 (w/w), is added to the previous solution and left stirring for 1h. This solution is dialized for 24 hours.

For calculating the concentration of the solution of iron oxide it was used a spectrophotometer AnalytikJena Specord 205 to obtain the value of the absorbance of the solution. The next equation relates the absorbance and the concentration of the solution:

$$A = K.c \tag{4.1}$$

where is an internal parameter related to the length of the distance that light passes trought in the spectometer and the absorptivity, valued in K = 0,193 L/mg. After calculation, the final value of the concentration of iron oxide was 11,23 mg/mL.

#### 4.2.3.2 Preparation of alginate solution

Iron oxide is embedded inside the alginate solution in order to separate these particles from the other substances, applying an external magnetic field. For this process, a solution of iron oxide and alginate 0,025% is prepared. The iron oxide used is the solution, diluted 1:2 (c= 5,62 mg/mL) and a solution of alginate 0,05% prepared previously, diluting 0,5g of alginate in 10g of deionized water (Figure 4.3).

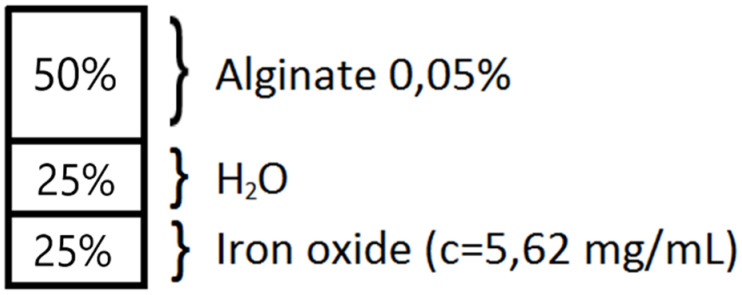


Figure 4.3: Percentage of iron oxide and alginate used for dispersed phase solution.

### 4.2.4 Preparation of continuous phase

Two continuous phases are prepared for this experiment, based on 1-undecanol. They are used in different moments of the microparticles productions.

- Continuous phase 1, composed by 1-undecanol with surfactant ABIL Em 90 (5% w/w);
- Continuous phase 2, consists in 1-undecanol with surfactant ABIL Em 90 (5% w/w) and 2% of calcium iodide;

### 4.2.5 Fabrication of microparticles in the microfluidic device

The schematic representation of the microfluidic device is illustrated in Figure 4.4. The flow focusing device consists of three inlets, one outlet, two junctions and expanding chamber. The continuous phases fluids are injected into the other inlets 1 (continuous phase 1) and 2 (continuous phase 2) while dispersed phase fluid is injected into the inlet 3. The three fluids are inserted through syringes (Hamilton 0.25 ml, Hamilton 5 ml, and Hamilton 2.5 ml, respectively) connected by teflon capillaries (ID 0.8 mm, OD 1.6 mm) and attached to the linear pumps (neMESYS 290N, Cetoni) to provide constant flow rate of each phase . Continuous phase 1 fluid flowing from two opposite sides of the channel brakes the dispersed phase at the junction, which lead to generating droplets at the orifice channel, or the expanding chamber.

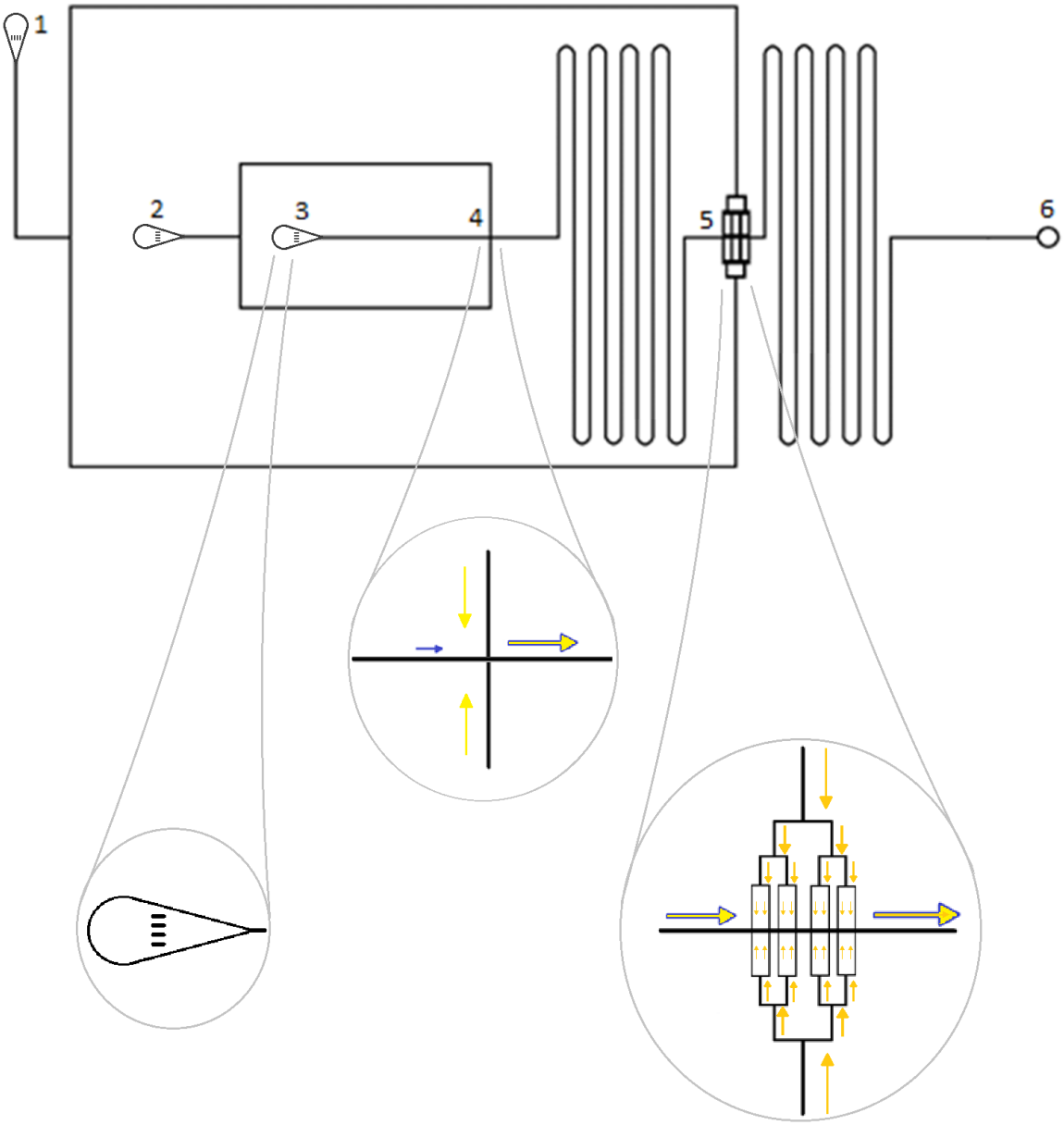


Figure 4.4: Microchip scheme: 1-input of oil with Ca+; 2- input of oil; 3 input of alginate solution; 4- mixture between oil and alginate; 5- solidification of microparticles by addition of oil with Ca+; 6- output of particles

Initially, all capillaries were filled with an appropriate solution, to prevent the formation of bubbles inside the chip. For all experiments and the reliability of the results of each test, the device is continuously operated for 10 min with constant flow rate, and then the results of the experiments are recorded. The experiments are monitored by an inverted microscope. Continuous Phase I meets the dispersed and droplets are formed (see Figure 4.4-4). In the following wavy channel of the microfluidic chip, diffusion of water into 1-undecanol occurs, leading to a reduction in the size of the aqueous droplets. Thereafter, the flow of calcium ions is introduced into the fluid flow as Phase II continuous (Figure 4.4-5). In the following wavy channel, the reticulation and gelation of alginate occurs, leading to the formation of solid alginate microparticles.

### 4.2.6 Particles modification

The last part of the process was to modify the particles so that they are ready for future use in target delivery.

#### 4.2.6.1 Chitosan stabilization

Chitosan was used for creating complexes alginate-chitosan by electrostatic interaction between the anionic residues of alginate and a positively charged amino terminals of chitosan. In this way, the structure of the microparticles became more stable. After cleaning with pure 1-undecanol and later with water, the particles were decanted using a magnet, taking advantage of the magnetic properties of the iron oxide. Meanwhile, a 1% (w/w) chitosan solution was prepared into 1% (w/w) acetic acid solution. Finally, the particles were transferred to the chitosan solution and stirred for 24h.

#### 4.2.6.2 Glutaraldehyde cross-linking

In order to provide copolymer properties, a cross-linking agent was added to the surface of the particles (Figure 4.5. After stabilizing the particles with chitosan, they were washed with PBS ( phosphate buffer saline) solution, transferred into 1 ml of glutaraldehyde solution (10% v/v) and incubated (Eppendorf ThermoMixer C) for 1 hour (25 ℃, 1 000 rpm). Afterwards, the particles were washed three times with PBS solution.

A different cross-linker could be also used for the modification since it depends on which group is going to react during the bonding process. In this case, the hydroxyl groups of the glutaraldehyde are the responsible for the bonding.

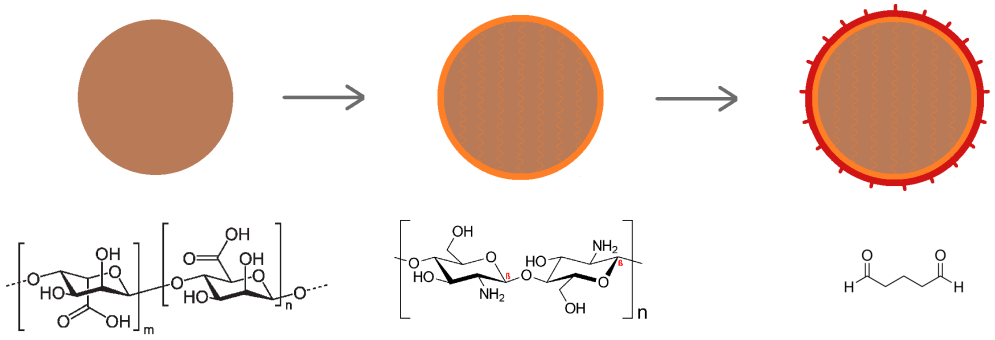


Figure 4.5: Modification process: Stabilizing the alginate microparticle shape with chitosan and cross-linking with glutaraldehyde as cross-linker

### 4.2.7 COMSOL Multiphysics simulation

In this study, the microfluidic chip designed above was modeled using the finite element method. The necessary procedures have been made to analyze the microfluidic chip designed using the COMSOL Multiphysics.

By using COMSOL Multiphysics tests and analyzes will be made. These analysis give the desired analysis and results to the user without producing the microchip. In the COMSOL Multiphysics program, it is possible to make many analyzes related to physics parameters.

This steps were followed in order to simulate microfluidics in COMSOL Multiphysics:

- Geometry modeling. According to the subject's shape and the condition of microfluidics, a model 2D of the flow focusing cross section in designed in CorelDRRAW and established in COMSOL;
- Physics settings. Physics menu contains two settings, which are subdomain settings and boundary settings. Subdomain settings is for setting each domain's material property, initial conditions etc. Boundary settings is for setting boundary conditions in two aspects. Firstly, it can set boundary conditions on the interface of different materials. Secondly, it can also set boundary conditions on the interface between material and the environment;
- Solving. COMSOL Multiphysics's solver can be selected for dealing with different problems. Users can either select the proper solver according to their problem or use the default setting. Refers to this thesis, the author use the default setting to solve the three heat transfer problems;

And the following input parameters specify the behavior of the dispersed phase in the continuous phase and the flow rate of each input, which are;

- Pressure input in the continuous phase microfluidic channel;
- Pressure input in the dispersed phase microfluidic channel ;
- Velocity inlet of the continuous phase to the microfluidic channel;
- Velocity inlet of the dispersed phase to the microfluidic channel;
- Surface tension of the continuous phase;
- Surface tension of the dispersed phase;

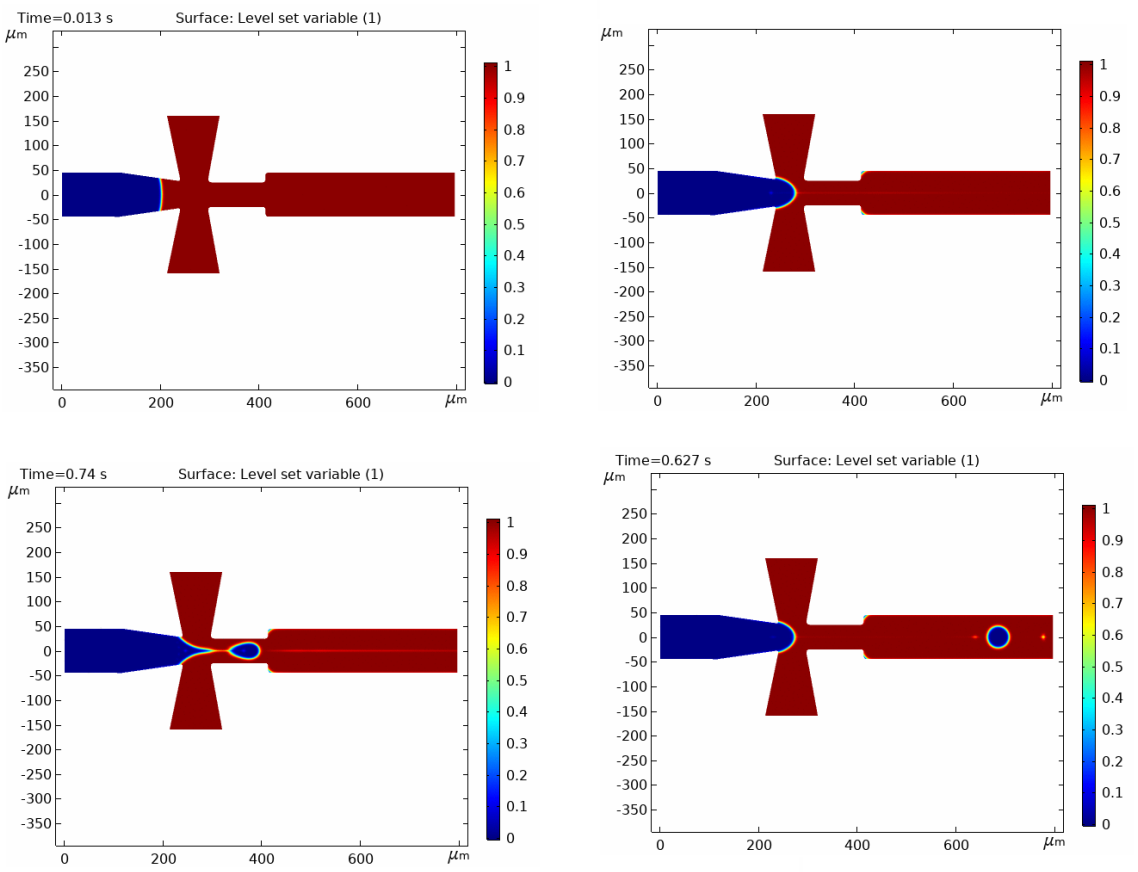


Figure 4.6: Simulation with COMSOL Multiphysics of a flow focusing cross-junction microfluidics with alginate solution as dispersed phase and 1-undecanol as continuous phase.

It is possible to compare the mathematical models with the results obtained in the experiment, regarding the flow of alginate and oil (Figure 4.6).

The cross-junction was simulated by COMSOL Multiphysics. At this point two liquids interact: the continuous phase, 1, in red and the dispersed phase, 2, in blue. Among them there is the oil-water interphase, which is important for the formation of particles.

# Chapter 5

# Results and discussion

## 5.1 Dependence between drop size and flow rate

Figures 5.1 and 5.2 show series of images taken from the monodispersed droplet formation experiments, with each image corresponding to different oil flow rate. In this assay, the total aqueous flow rate was fixed at 10 $\mu$l/h.

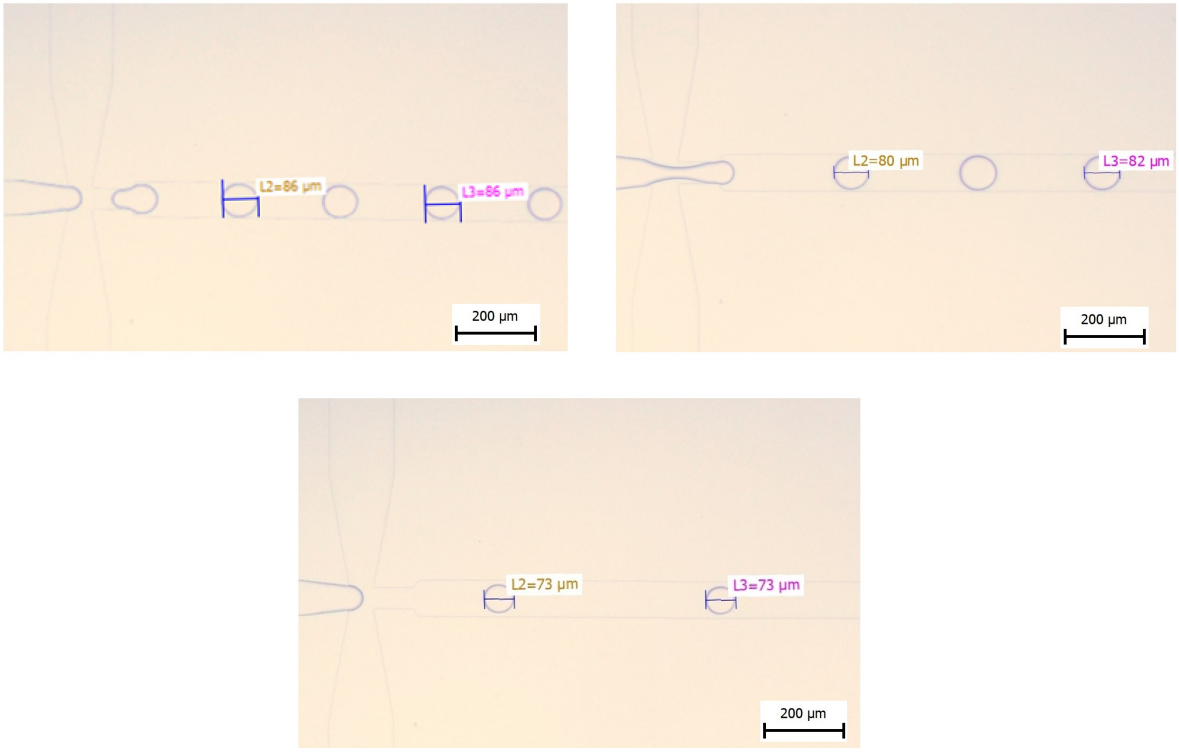


Figure 5.1: Images of droplet formation for different oil phase flow rates. The total aqueous phase was kept at 10 $\mu$l/h. While the oil assumes values of 70 $\mu$l/h (top left), 80 $\mu$l/h (top right) and 110 $\mu$l/h (bottom).

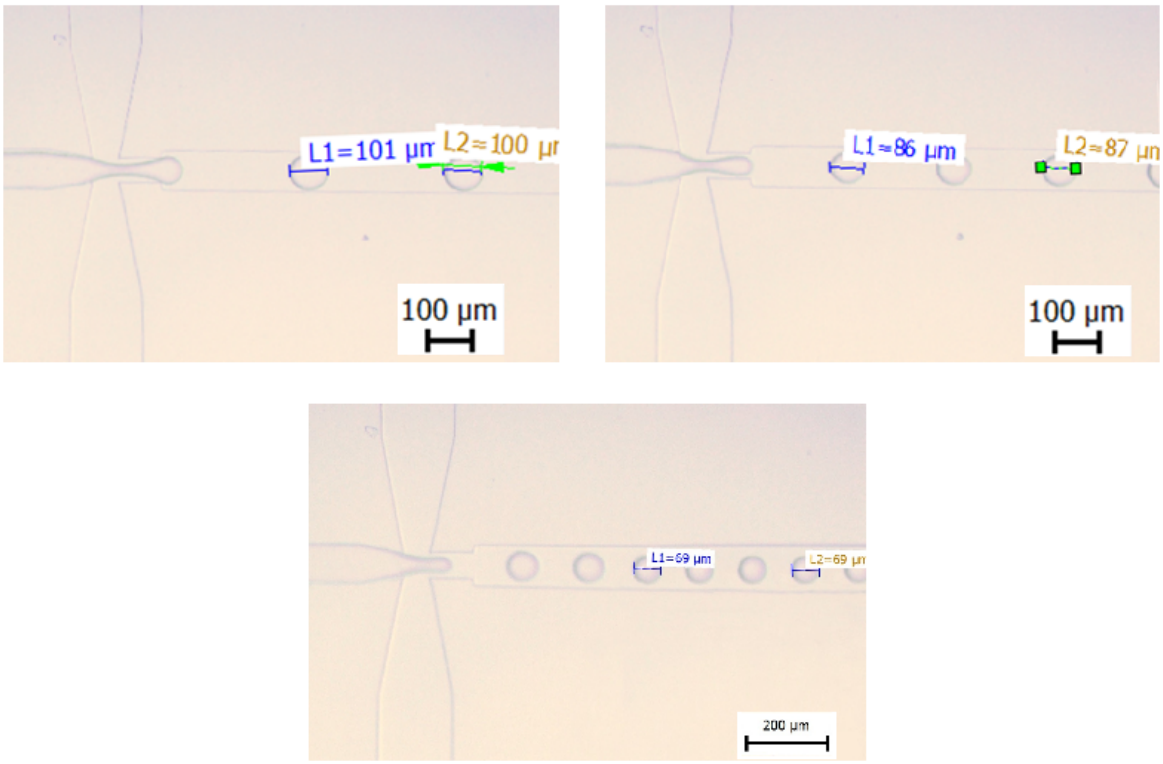


Figure 5.2: Images of droplet formation for different oil phase flow rates. The total aqueous phase was kept at 8 $\mu$l/h. While the oil assumes values of 40 $\mu$l/h (top left), 60 $\mu$l/h (top right) and 90 $\mu$l/h (bottom).

The particle diameter (d) was measured from the images using the imaging processing software QuickPHOTO MICRO 3.2. Only data in the range of 60-110 $\mu$l/h are shown in Figure 5.1. It can be seen that the increase of oil flow reduced the drop size.

In shear driven flow, the capillary number is important for determining the size of the droplet after breakup. The capillary number, Ca=$\mu$u/$\sigma$, is defined as the ratio of shear stress exerted on the droplet and interfacial tension of the droplet, where $\mu$ is the dynamic viscosity of the oil phase, u the characteristic of the fluid and $\sigma$ is the interfacial tension between water and oil interface.

In this device, since droplet breakup occurs at the orifice when the neck of the droplet becomes a singular point, where the cross-sectional area of the neck is small compared to the cross-sectional area of the channel, the shear rate generated by the oil phase can be approximated as the velocity of the oil flow divided by the width of the channel, since the dispersed phase flow rate is negligible compared to the oil phase.

In Figure 5.3, the drop size as a function of the flow rate shows the variation with a constant flow rate of the dispersed phase, in different assays . At the lowest flow rate ratios the drop sizes are nearly on the order of the flow focusing orifice size, d/D$\approx$1, which indicates the geometric control of drop size common to many microfluidic experiments.

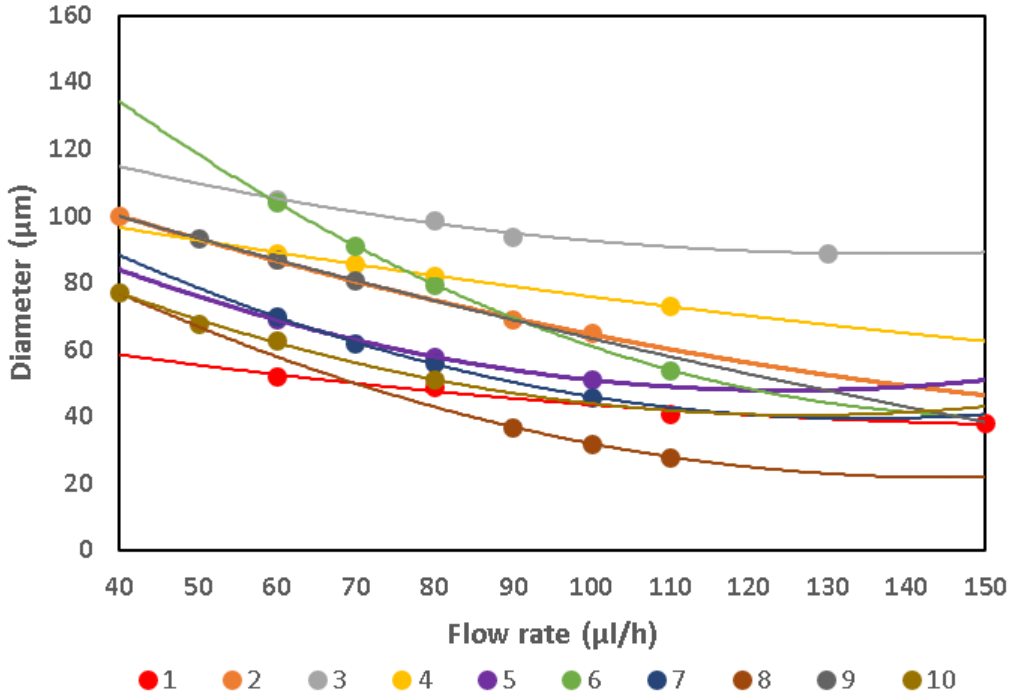


Figure 5.3: Droplet diameter versus flow rate of the oil, for a constant dispersed phase flow rate.

For each test, it was added a trend line that adjusted better to the points (Figure 5.3). In all cases, a quadratic function fit well, with a $R^2$ greater than 0,98. The decrease in particle diameter is between 4,8 and 14% for each increment of 10 $\mu$m in the continuous phase flow rate, depending on the initial flow rate of the continuous phase.

The quadratic functions are defined by $\mathbf{a}x^2+\mathbf{b}x+\mathbf{c}=0$ where each variable **a**, **b**, **c** have a different role in the standard form of the quadratic functions.

- The value of **a** changes the width of the opening of the parabola and that the sign of **a** determines whether the parabola opens upwards or downwards.
- The value of **b** moves the axis of symmetry of the parabola from side to side; increasing b will move the axis in the opposite direction.
- The value of **c** moves the vertex of the parabola up or down and **c** is always the value of the y-intercept.

In this experiment, the variable b and c is related to the particle size, which depends on the dispersed phase flow rate used for each assay. On the other hand, the variable **a** represents the variation of the particle size for different flow rates.

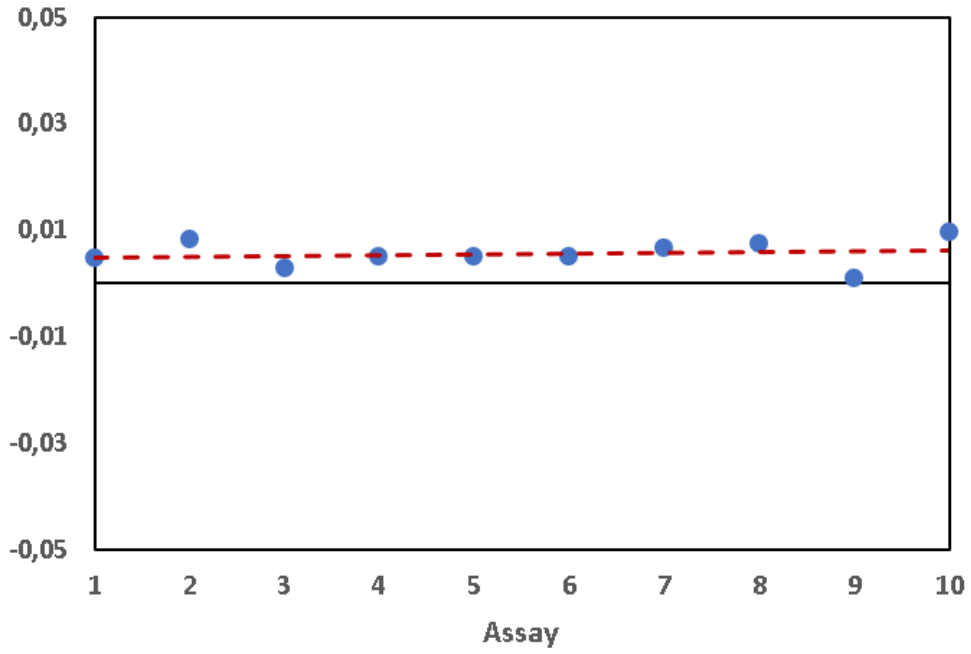


Figure 5.4: Comparation between the **a** constant of different assays, with aqueous solution flow rate constant.

It can be seen, that the value of a oscillates around the value of **a**$\approx$ 0,0056 (Figure 5.4). That means that, knowing the size of some particles, specifically. With a couples of particles, **B** and **C**, with diameter **b1** and **c1**, produced with a oil flow rate **b2** and **c2**, respectively, is possible to obtain an estimated value of the particle diameter for every oil flow rate.

$$d(x) = ax^2 + (\omega - a)x + 15(\omega - 2a) + c1 \tag{5.1}$$

with $\omega = \frac{b1-c1}{b2-c2}$.

A similar experiment was done with the dispersed phase. In this case, for each assay the flow rate of continuous phase has a constant value, meanwhile the flow rate of the dispersed phase is varying along the assays (Figure 5.5 and Figure 5.6).

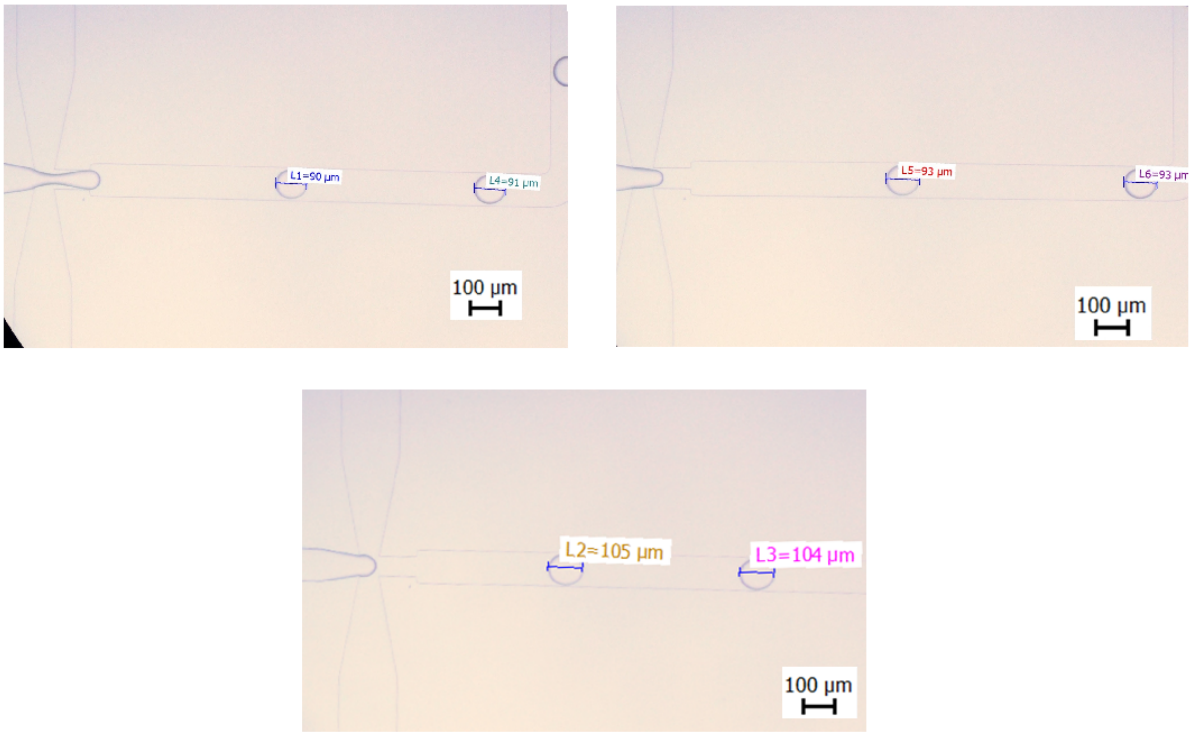


Figure 5.5: Images of droplet formation for different aqueous phase flow rates. The total aqueous phase was kept at 60 µl/h. While the solution assumes values of 11 µl/h (top left), 12 µl/h (top right) and 15 µl/h (bottom)

.

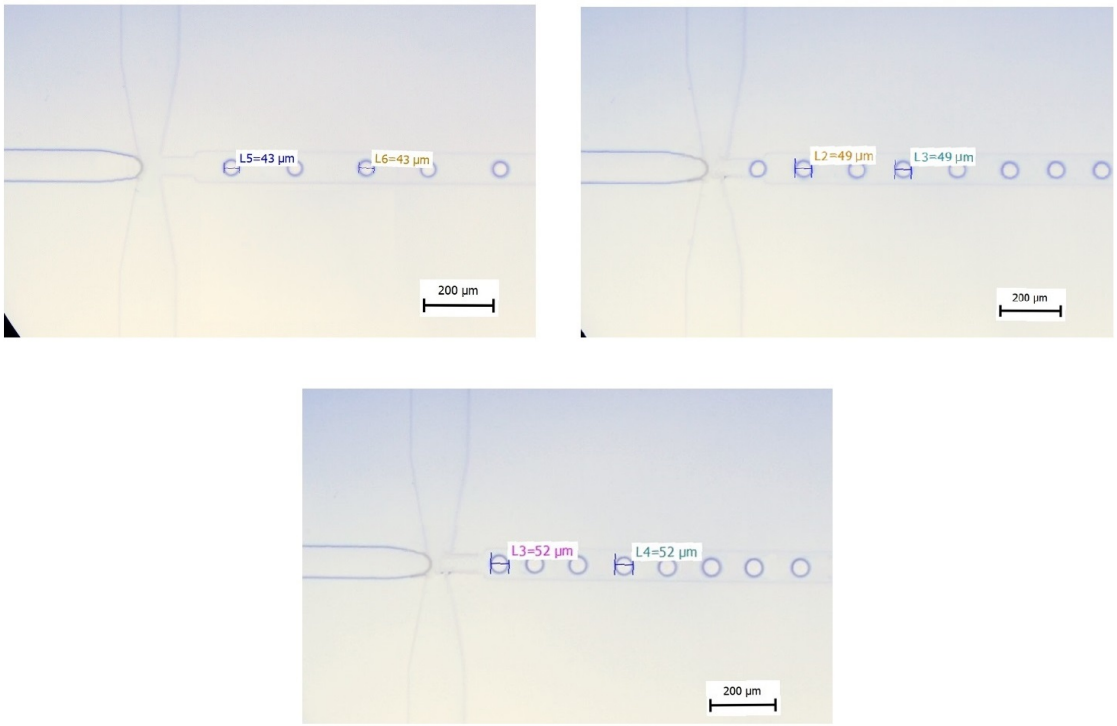


Figure 5.6: Images of droplet formation for different aqueous phase flow rates. The total aqueous phase was kept at 150 µl/h. While the solution assumes values of 5 µl/h (top left), 9 µl/h (top right) and 11 µl/h (bottom)

.

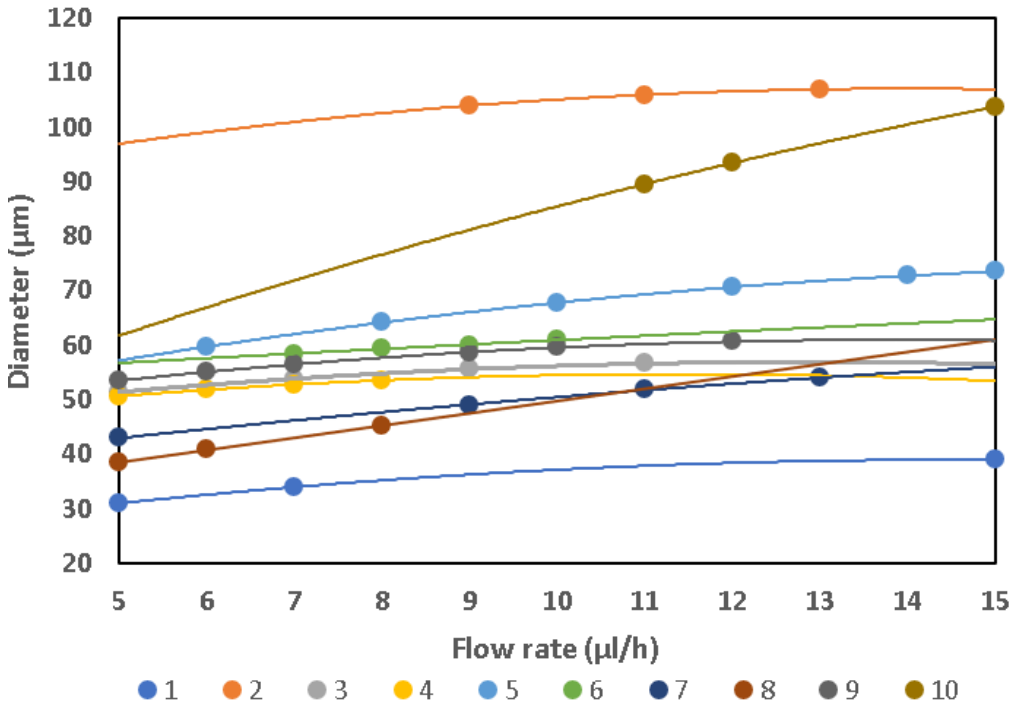


Figure 5.7: Droplet diameter versus flow rate of the aqueous solution, for a constant continuous phase flow rate.

In this case, the increase of particle diameter is between 0,5 and 4% for each increment of 1$\mu$l/h in the flow, depending on the initial flow of the dispersed phase (Figure 5.7). And as with oil, a quadratic regression was performed for each of the tests. From these assays, the constant **a** was obtained and compared (Figure 5.8).

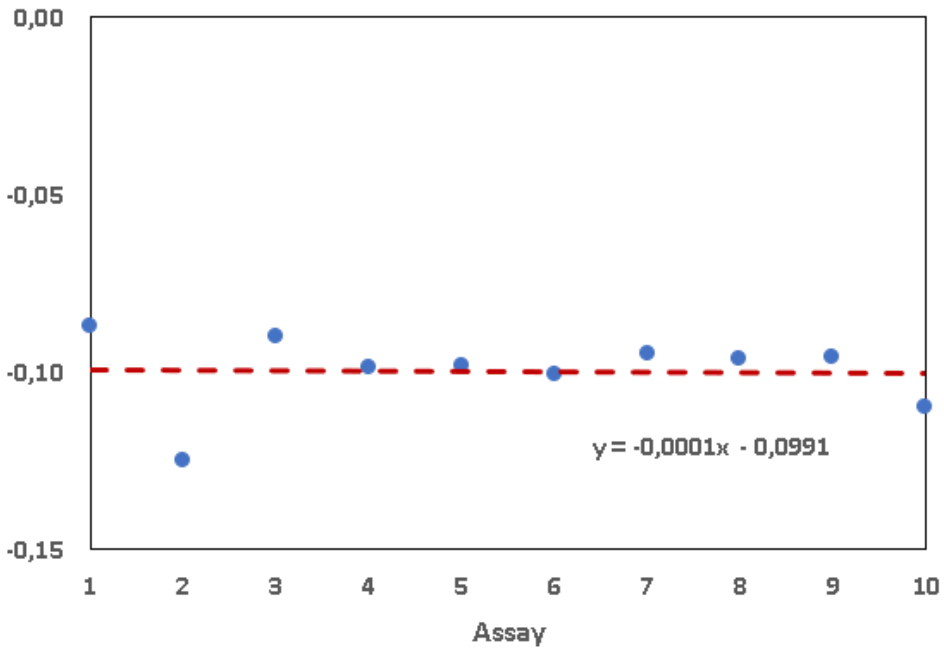


Figure 5.8: Comparation between the **a** constant of different assays, with oil flow rate constant.

The value of **a** oscillate around ≈-0,10.

### 5.1.1 Size along the chip

Besides the flow focusing, there are other key points along the microchip. Points like the wavy channels for extraction of water, continuous phase II input to the device and wavy channels for cross-linking of alginate droplets (gelation) were also compared (Figure 5.12 and Figure 5.10), for a constant flow rate of all inputs phases.

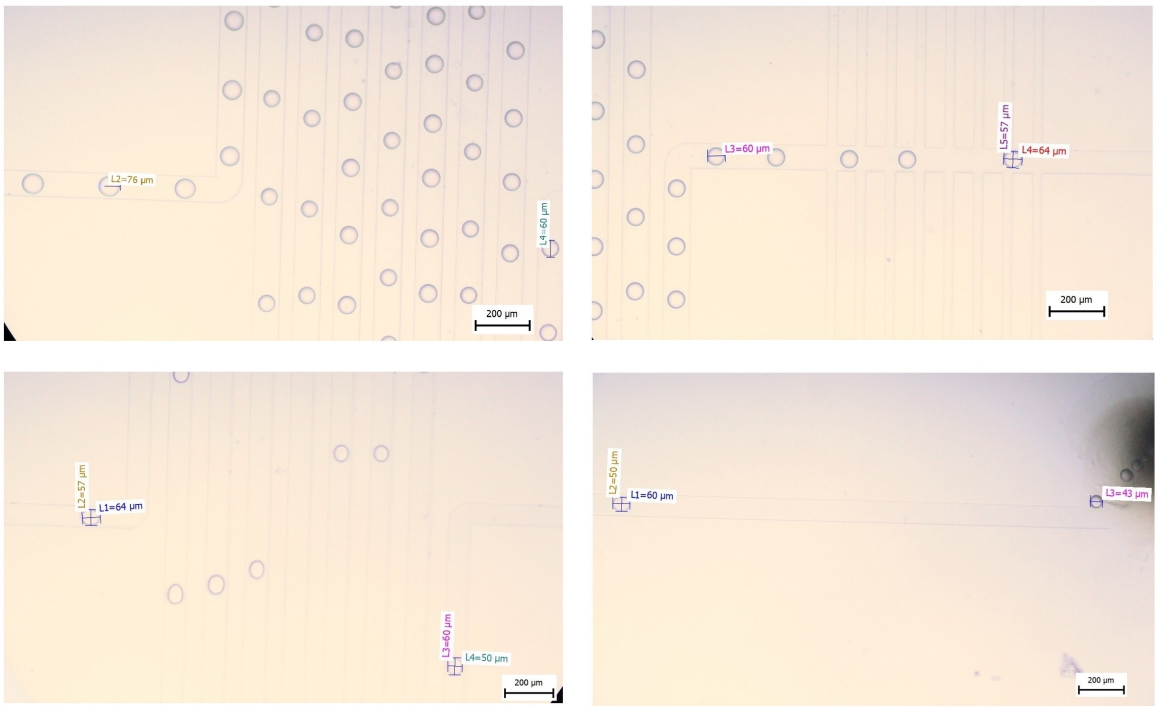


Figure 5.9: Pictures of the microfluidic device with different stages of particles preparation: Extraction of water from the droplets into the oil phase (top left), entry of the continuous phase II into the device (top right),gelation of the droplets due to the calcium ions included in continuous phase II (bottom left) and outlet of the particles from the device (bottom right), for a flow rate of 76 $\mu$l/h after flow focusing.

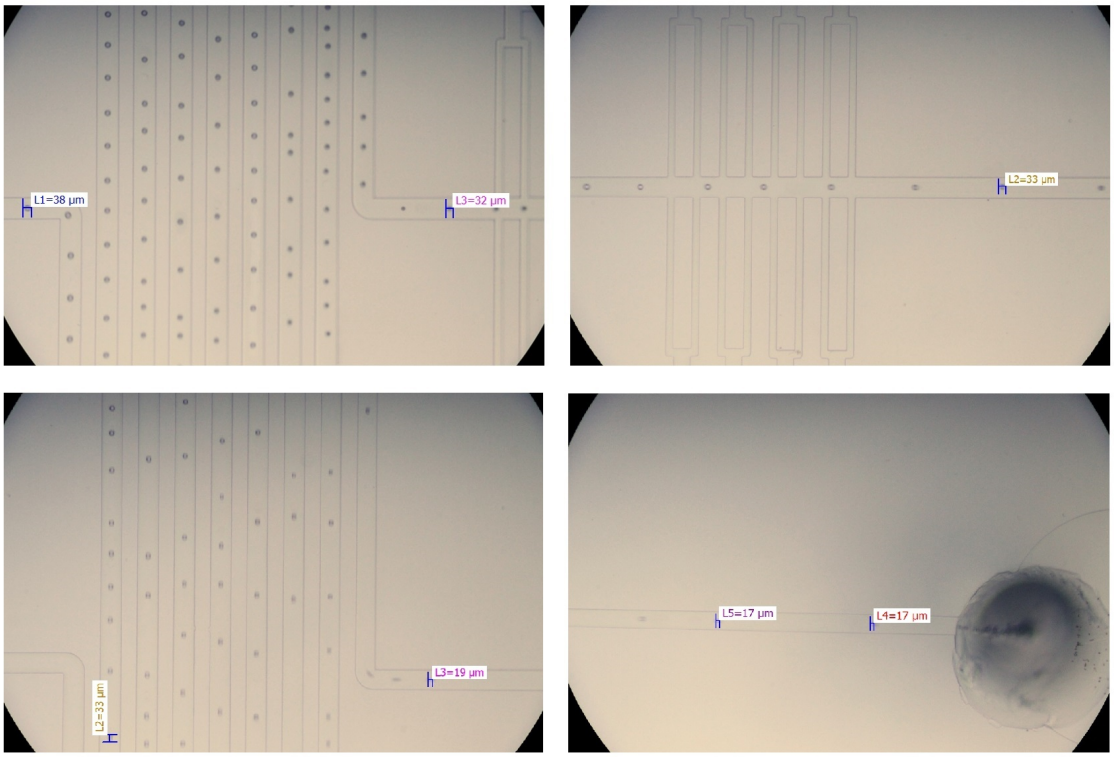


Figure 5.10: Pictures of the microfluidic device with different stages of particles preparation: Extraction of water from the droplets into the oil phase (top left), entry of the continuous phase II into the device (top right), gelation of the droplets due to the calcium ions included in continuous phase II (bottom left) and outlet of the particles from the device (bottom right), for a flow rate of 38 $\mu$l/h after flow focusing.

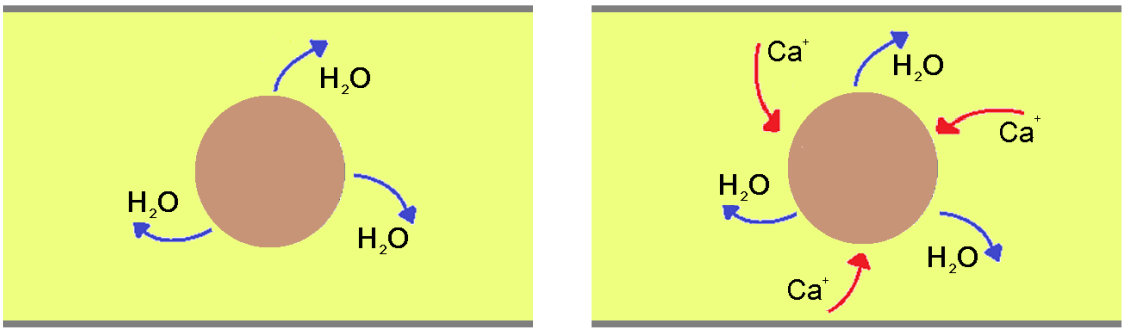


Figure 5.11: Illustration of the diffusion of water particles after the addition of continuous phase I (on the left) and cross-linking with Ca+ after continuous phase II (on the right).

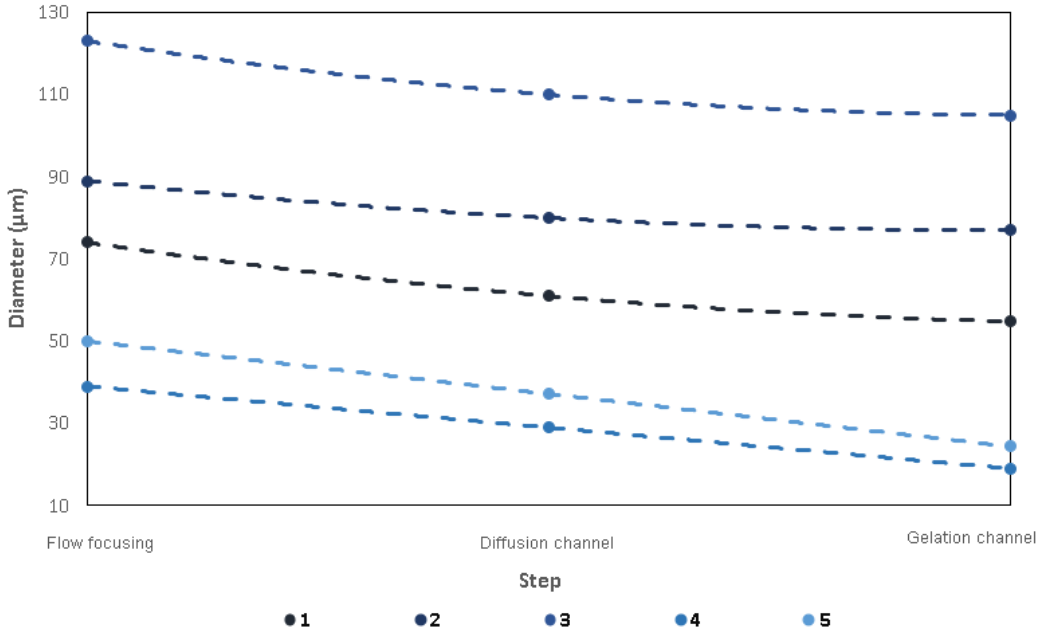


Figure 5.12: Graphic showing the decreasing of the size for different steps into the microchip, for different assays. The step 1 is after the continuous phase I addition in the flow focusing part, the step 2 is after the diffusion of water in the first wavy channel where occurs the diffusion of water in oil and the step 3 is after the gelation of the particles caused by cross-linking with Ca+ and diffusion of water in the second wavy channel.

As it is possible to see in Figure 5.12, the particle size decreases along the microchip, specially after the two wavy channel. It is caused because of the diffusion (Figure 5.11) of some water particles into continuous phase and the cross-linking and gelation. Between the flow focusing junction and the end of the diffusion channel, in average, the particles decrease 12%. Meanwhile between the end of diffusion channel and the end of gelation channel the is a decreasing of 6% on the size of the particle.

In some cases, at points of velocity increasing of the continuous phase, such as in the flow focusing junction or during the input of continuous phase II, the particles can get flatter, acquiring more elliptical shape than spherical. Visually, the particles seem to have a different shape than before the increasing of the flow rate. In the first case, in the first case, the continuous phase flow goes from null to significantly higher. In the second case, the flow of the continuous phase is the sum of the oil flow and oil with added calcium iodide.

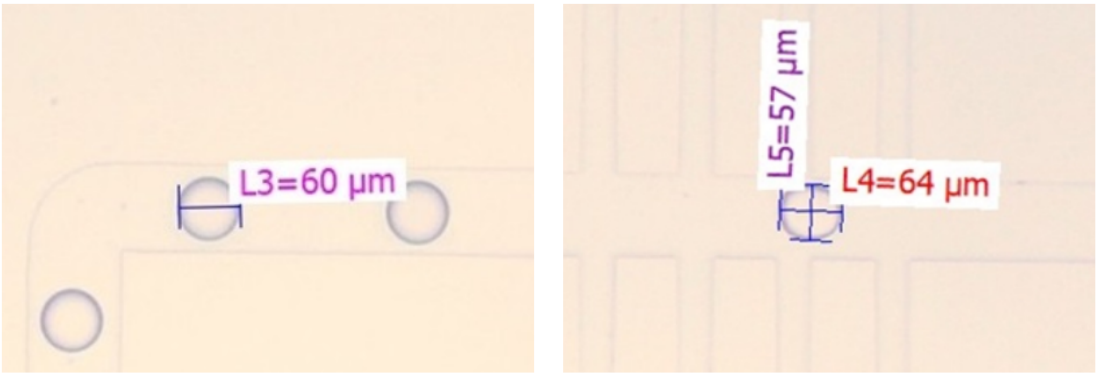


Figure 5.13: Image comparing particles size before and after addition of the continuous phase II input. After the particles passes through this point, the flow rate of the continuous phase is the sum of the flow rates of the continuous phase I and II.

However, since the thickness of the channels are minimal $\lessapprox 9$ $\mu$m, the size of the particles can be compared just taking in account their area. Through calculations it is possible to verify that the particle size is practically the same as the initial one.

$$Areao f circle = r^2\pi \tag{5.2}$$

$$Areao f ellipse = ab\pi \tag{5.3}$$

where r is the radius of a spherical particle. The values a and b are the length and width of the particle, respectively, after speeding up (Figure 5.13). Using the values of Figure 5.13 on the equations 5.2 and , the values of the areas obtained are 11309,73 and 11460,52, with a relative error of 1,33%.

### 5.1.2 Surface modification of microparticles

After producing the particles, they are modified for using them as targeted delivery particles, so the effect of particle modification was studied. Chitosan solutions with concentration 1% was tested for different curing times: 15 minutes, 1 hour and 6 hours (Figure 5.20).

The modification is done in acetic acid solution environment. The average diameter of the particles prepared had decreased significantly.


Figure 5.14: Pictures of the particles after modification with chitosan with different curing times: 15 min (top left), 1h (top right) and 6h (bottom).

From 15 min to 1h there is a decreasing of 17% in the size of the particle and 27% from 1h to 6h.

### 5.1.3 Effect of iron oxide

The particles obtained with coated iron oxide have potential in medicine, particularly as magneto-responsive drug delivery carriers. It is possible to control the movement of magnetic particles in the biological object by external magnetic field. In addition, iron oxide nanoparticles can be used as a local source heat in the presence of an alternating magnetic field in the radio frequency band.

During the modification, the iron oxide used in the preparation of the alginate solution gives an advantage when handling them. due to easy and faster decantation.

Figure 5.15: Pictures of particles under influence of a magnetic field.

The alienation of the particles are a response of the particles to the magnetic fields since it is energetically favorable (Figure **??**). In the corrugated configuration, the magnetic field is concentrated in the aggregation of particles. They are more easily magnetized than the aqueous medium, this lowers the magnetic energy.

### 5.1.4 Model Analysis

The particle diameters obtained experimentally were compared with the simulation in COMSOL Multiphysics, for the same flow rate of the continuous and dispersed phase (Figure 5.16).

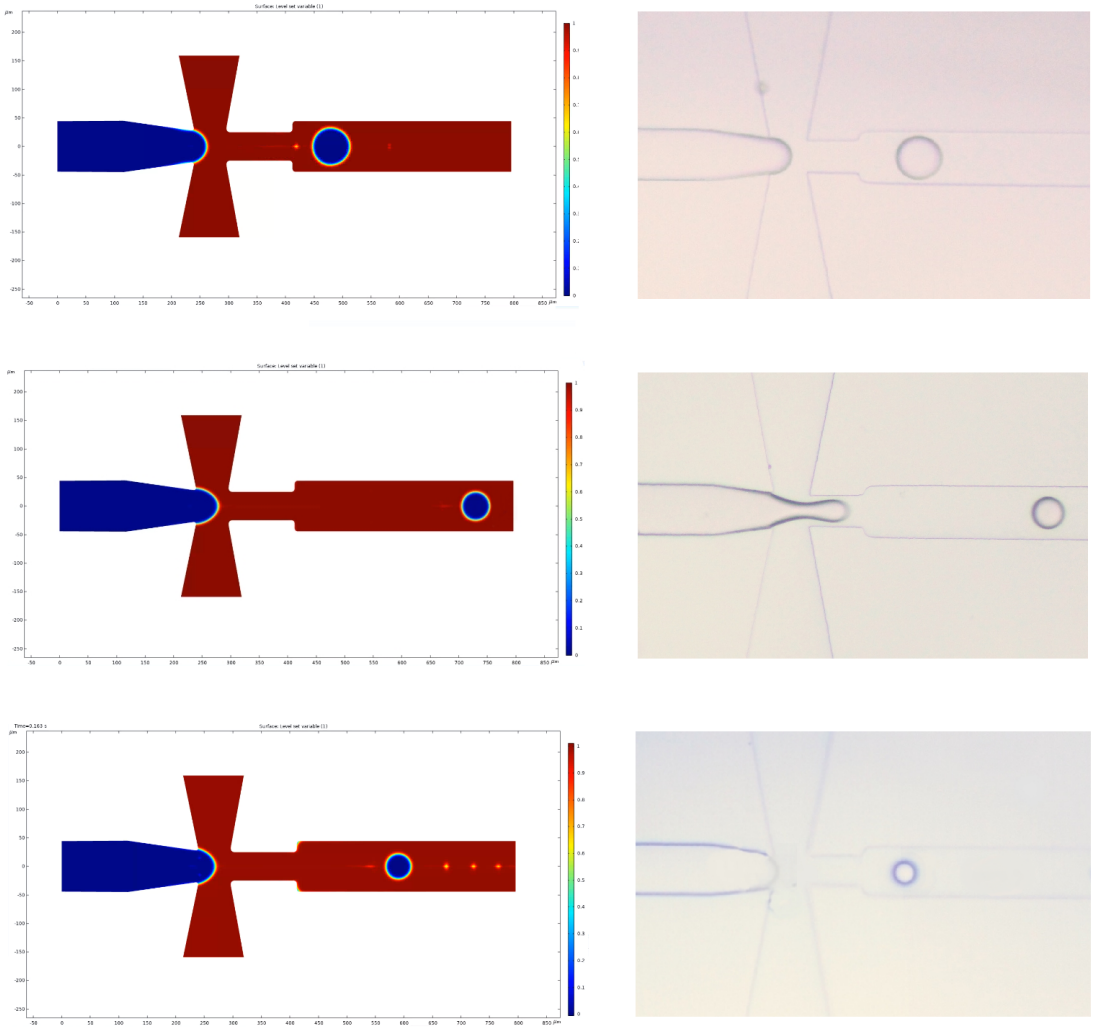

Figure 5.16: Comparison between simulated and experimental particles for values of flow rates of continuous and dispersed phase of 70 and 7 $\mu$l/h (assay 1, top), 120 and 5 $\mu$l/h (assay 2, middle), 150 and 5$\mu$l/h (assay 3, bottom), respectively.

| Assay | Simulated diameter ($\mu$m) | Experimental diameter($\mu$m) | Error(%) |
|---|---|---|---|
| 1 | 67 | 69 | 2.9 |
| 2 | 49 | 52 | 6.1 |
| 3 | 40 | 41 | 2.5 |

Table 5.1: Table comparing the diameter of the particles obtained experimentally and using COMSOL Multiphysics.

The relative error between the simulation and the values obtained experimentally are $\leq$7% (Table 5.1).

The influence of the continuous phase flow rate changing can be also compared. The flow of alginate was kept constant at 5 $\mu$l/h, while the flow of oil was changed for each simulation. Thus, the Figure 5.17 is obtained.

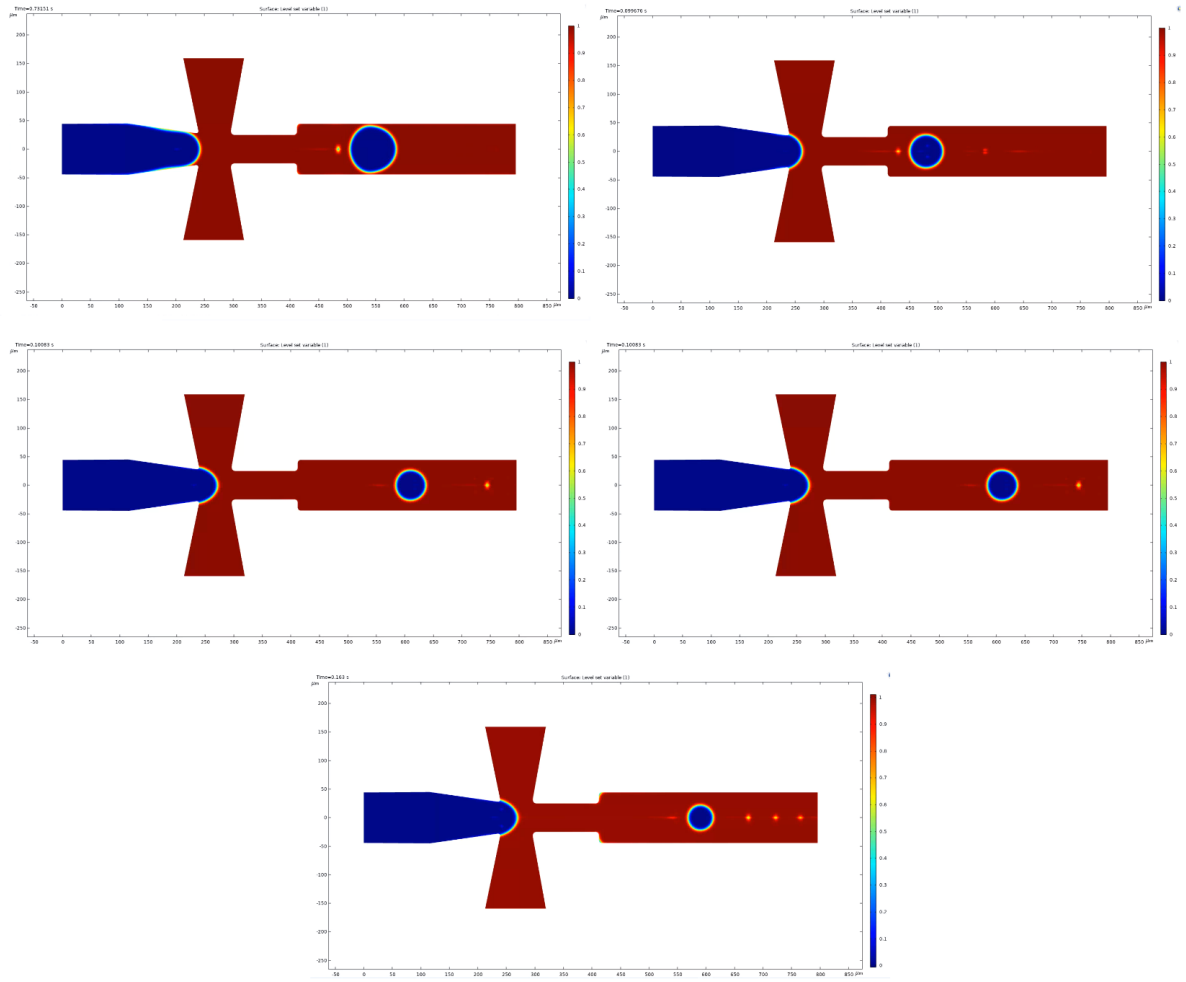

Figure 5.17: Simulation of microfluidics system by COMSOL Multiphysics, with dispersed phase constant. Flow of continuous phase: 60 $\mu$l/h (top left), 80 $\mu$l/h (top right), 100 $\mu$l/h (middle left), 120 $\mu$l/h (middle rigth), 150 $\mu$l/h (bottom)

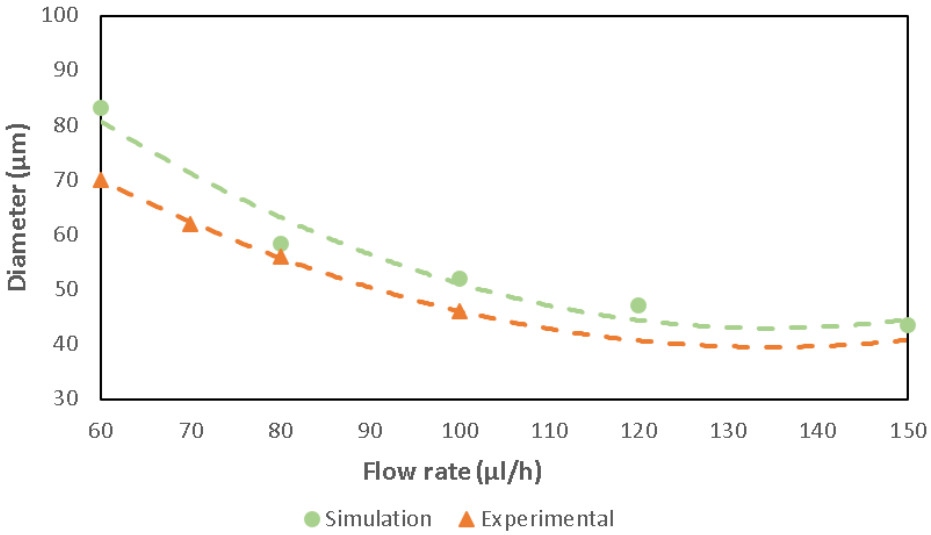


Figure 5.18: Comparison of the size of the particles produced for different flow rate of continuous phase.

From the Figure 5.18 is possible to obtain decreasing percentage of the diameter of the particles per 10 $\mu$l/h increase of the flow continuous flow rate and compare it with the values obtained experimentally. They vary between 4,1% and 14% depending of the flow. The constant **a** was also obtained from the simulation in order to predict the six of the particles obtained for higher and lower flow rates. The constant **a** have a value of -0,0068, 18% lower than the value obtained experimentally (Table 5.2).

Table 5.2: Comparison between the percentage of variation and the value of **a** for experimental assay and simulation, for oil flow rate increasing.

| | Variation per 10$\mu$l/h (%) | Value of **a** |
|---|---|---|
| Experimental | 4,8-15 | 0,0056 |
| Simulation | 4,1-14 | 0,0068 |

The influence of alginate flow rate was also studied in the COMSOL simulation (Figure 5.19).

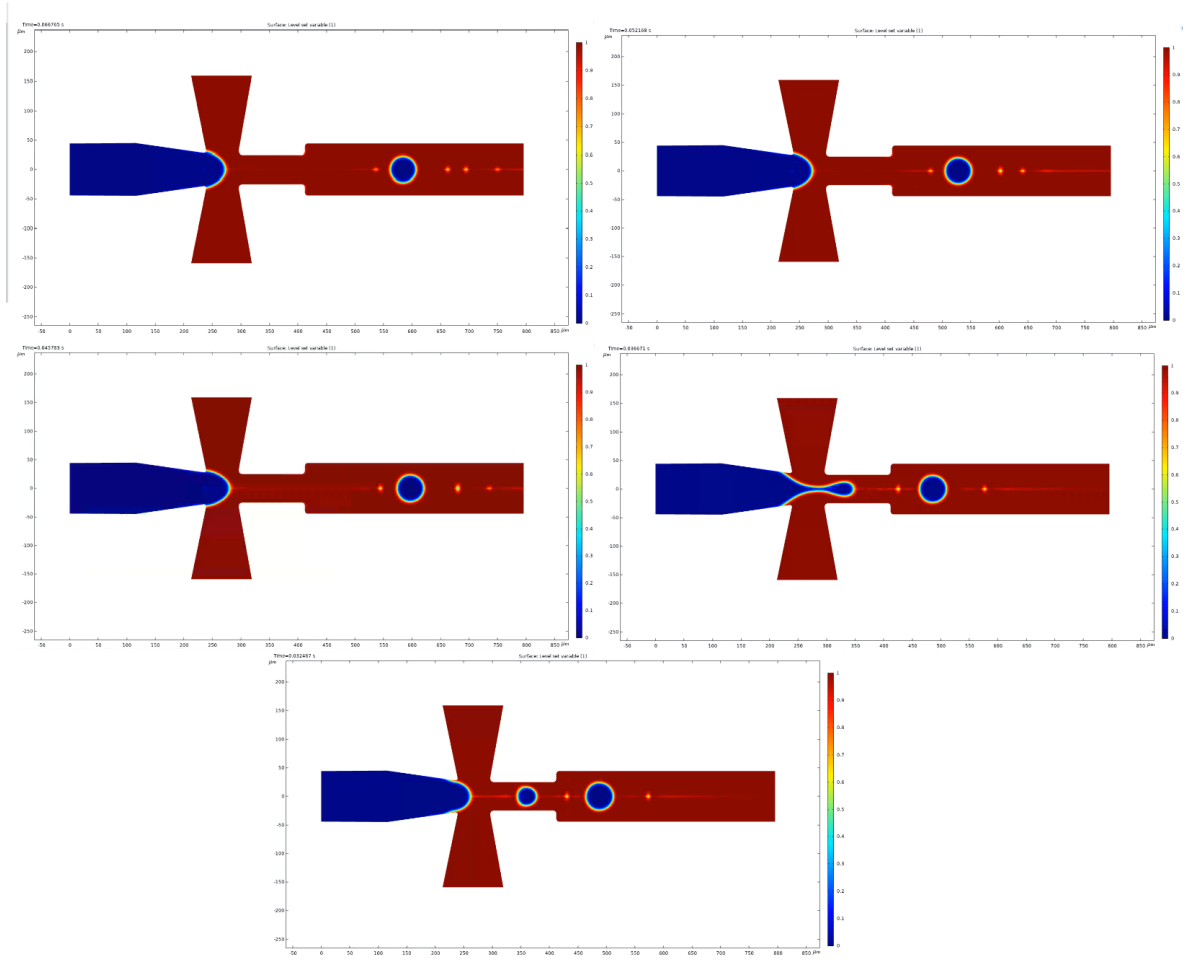

Figure 5.19: Simulation of microfluidics system by COMSOL Multiphysics, with continuous phase constant. Flow of continuous phase: 7 $\mu$l/h (top left), 9 $\mu$l/h (top right), 11 $\mu$l/h (middle left), 13 $\mu$l/h (middle rigth), 15 $\mu$l/h (bottom)

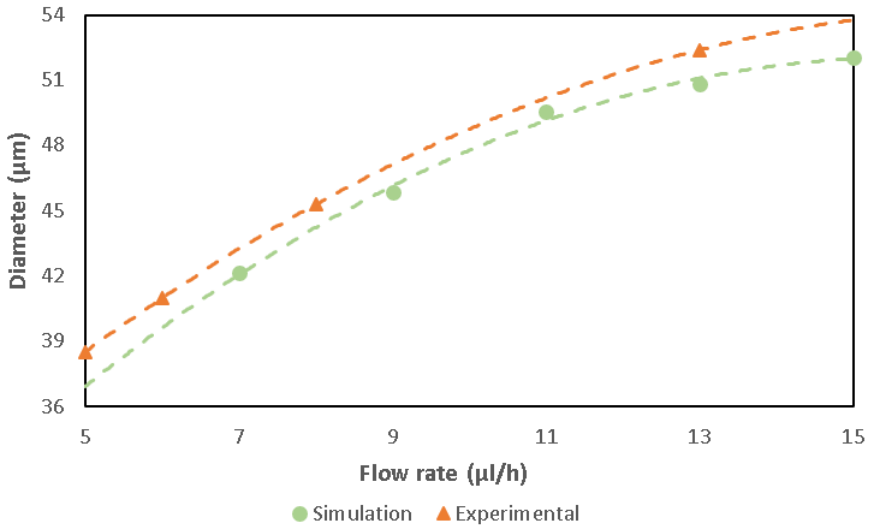


Figure 5.20: Comparison of the size of the particles produced for different flow rate of dispersed phase.

As the previous simulation, the value of the size change percentage was obtained as well as the value of **a**. The particles diameter decrease between 1,2% to 4,4% for each 1 $\mu$l/h increasing (Figure 5.20) of the dispersed flow rate and the value of **a** is 0,12, 16% lower than the value obtained experimentally (Table 5.3).

Table 5.3: Comparison between the percentage of variation and the value of **a** for experimental assay and simulation, for alginate flow rate increasing.

| | Variation per 1$\mu$l/h (%) | Value of **a** |
|---|---|---|
| Experimental | 0,5-4,0 | -0,10 |
| Simulation | 1,2-4,4 | -0,12 |

# Chapter 6

# Conclusion

The field of microfluidics has made tremendous strides in recent years with the majority of the effort focused on chemical analysis. Microfluidic devices are in many respects ideally suited to this task because they can be made at low costs relative to traditional instrumentation and are small and thus potentially quite portable.

The extractive gelation process was used for down-scaling the droplet volume produced in a flow focusing cross junction, and on-chip gelation with subsequent magnetic separation of the produced gel microparticles was employed as a separation and purification method.

First, microchips of PDMS microchips were fabricated using two ways of assembly of the parts of the microchip: taking advantage of the heat surface before total polymerization and using plasma surface activation. The easy assembly of microchip makes such tips suitable for versatile tests of chip prototypes. The robust nickel mould has been found useful in the numerous fabrications of PDMS microstructures.

The particles and microparticles, consisting of alginate and iron oxide nanoparticles, were prepared in different flow rates. The rate of variation of the particles was studied increasing the flow rates of the continuous phase or the dispersed phase. A second degree trend line was modeled to each set o values, from which parameter **a** of the polynomial equation was obtained. As well as the rate of increasing or decreasing of the particles, depending on the flow rate of alginate solution (0,025% w/w) with iron oxide (c=5,6 mg/mL) and 1-undecanol with 5% w/w of surfactant ABIL.

The particle sizes were also compared for each position in the microchips, especially at points of increase or decrease in speed. From these values, the rate of decrease of the particle was obtained. Either after the addition of 1-undecanol with ABIL, in which water diffuses into the oil, as after the addition of 1-undecanol with ABIL and CaI (2% w/w).

Later, the microchip shape designed in CorelDRAW was loaded to the simulation software COMSOL Multiphysics and a simulation of the flow focusing cross junction was done. It is the one of the most important point of the microchip since from this point will depend the size and shape that the particle will adopt along the microchip. Through this simulation, several simulations were made to compare these values with the values obtained experimentally: the rate of variation of the diameter of the particle and the constant **a** of the trend line.

# Bibliography


[1] Fluigent, "WHAT IS THE HISTORY OF MICROFLUIDICS?." https://www.fluigent.com/microfluidic-expertise/what-is-microfluidic/history-of-microfluidics/, last accessed on 2020-12-09.

[2] Fluigent, "MICROFLUIDICS DEFINITIONS AND ADVANTAGES." https://www.fluigent.com/microfluidic-expertise/what-is-microfluidic/microfluidic-definitions-and-advantages/, last accessed on 2020-12-09.

[3] C. J. L. B. L. G. H. M. U. C. N. Bruce K. Gale, Alexander R. Jafek and S. K. Kamarapu, "A Review of Current Methods in Microfluidic Device Fabrication and Future Commercialization Prospects," *Microfluidics and Nanofluidics*, vol. 3, no. 60, 2018.

[4] G. M. Whitesides, "The origins and the future of microfluidics," *INSIGHT OVERVIEW*, vol. 442, 20106.

[5] P. Zhu and L. Wang, "Passive and active droplet generation with microfluidics: a review," *Lab on a Chip*, vol. 17, pp. 34–75, 2017.

[6] A. D. F. S. Z. C. G. C. M. M. Darren R. Link, Erwan Grasland-Mongrain and D. A. Weitz, "Electric Control of Droplets in Microfluidic Devices," *Microreactors*, vol. 45, pp. 2556—2560, 2006.

[7] H. T. Jinchen Sun, "Active droplet generation in microfluidics ," *Lab on a chip*, vol. 6, pp. 1285–1309, 2013.

[8] E. Thomée, "Magnetic fluids and microfluidics: A short review," *Microfluidics flow control*, 2017.

[9] Socialized Science, "Microfluidics and Dimensionless Numbers," 2016. https://www.socializedscience.com/hacking/microfluidics-and-dimensionless-numbers, last accessed on 2020-29-03.

[10] Oilfield Glossary, "Enhanced Oil Recovery." https://www.glossary.oilfield.slb.com/en/Terms/b/bond_number.aspx, last accessed on 2020-29-03.

[11] Kruss Scientific, "Weber number." https://www.kruss-scientific.com/services/education-theory/glossary/weber-number, last accessed on 2020-29-03.

[12] H. W. Z. B. H. W. R. L. Bingjie Wang, Pepijn Prinsen and J. Xuan, "Macroporous materials: microfluidic fabrication, functionalization and applications," *Chemical Society Reviews*, vol. 46, pp. 855–914, 2017.

[13] S. H. I. Ramalingam Sitaraman and N. R. Kuloor, "A Generalized Equation for Diffusion in Liquids," *Indian Instit. Science*, vol. 8, no. 2, pp. 198–201, 1963.

[14] S. T. L. A. R. A. T M Tran, Freeman Lan, "From tubes to drops: Droplet-based microfluidics for ultrahigh-throughput biology," *Journal of Physics D: Applied Physics*, vol. 46, no. 11, 2014.

[15] Lina Wu, "Droplet Microfluidics: T-Junction," 2018. https://openwetware.org/wiki/Droplet_Microfluidics:_T-Junction_-_Lina_Wu, last accessed on 2020-10-04.

[16] Elveflow, "Microfluidics: A general overview of microfluidics." https://www.elveflow.com/microfluidic-reviews/general-microfluidics/a-general-overview-of-microfluidics/, last accessed on 2020-14-04.

[17] Potomac, "Microfluidics – Polymers vs. Glass ," 2019. https://www.potomac-laser.com/material/microfluidics-polymers-vs-glass/, last accessed on 2020-14-04.

[18] Elveflow, "Materials for microfluidic device fabrication: a review." https://www.elveflow.com/microfluidic-reviews/general-microfluidics/materials-for-microfluidic-chips-fabrication-a-review-2017/, last accessed on 2020-14-04.

[19] O. C. J. Tae Kyung Kim, Jeong Koo Kim, "Measurement of nonlinear mechanical properties of PDMS elastomer," *Microelectronic Engineering*, vol. 88, no. 8, pp. 1982–1985, 2011.

[20] T. Fujii, "PDMS-based microfluidic devices for biomedical applications," *Microelectronic Engineering*, vol. 61-62, pp. 907–914, 2002.

[21] B. M. Mohammad Mastiani, Seokju Seo and M. Kim, "High-Throughput Aqueous Two-Phase System Droplet Generation by Oil-Free Passive Microfluidics ," *ACS Omega*, vol. 3, no. 8, pp. 9296––9302, 2018.

[22] H. S. K. Junyi Yao, Fan Lin and J. Park, "The Effect of Oil Viscosity on Droplet Generation Rate and Droplet Size in a T-Junction Microfluidic Droplet Generator," *Micromachines*, vol. 10, no. 12, 2019.

[23] N. John S. Razzano, Cohoes, "PROCESS FOR PRODUCING OCTAMETHYLTRSLOXANE ," 1996.

[24] M. J.Wacker, V.K.Parashar, "Influence of Oil Type and Viscosity on Droplet Size in a Flow Focusing Microfluidic Device," *Procedia Chemistry*, vol. 1, pp. 1083—1086, 2009.

[25] PubChem, 2020. https://pubchem.ncbi.nlm.nih.gov/, last accessed on 2020-09-09.

[26] "Dodecane," 2020. https://en.wikipedia.org/wiki/Dodecane, last accessed on 2020-09-09.

[27] J. Jiao and D. J. Burgess, "Ostwald ripening of water-in-hydrocarbon emulsions," *Colloid and Interface Science*, vol. 264, pp. 509—-516, 2003.

[28] W. Textmap, "Physical Properties of Alkanes," *Organic chemistry*, vol. 4, no. 2, pp. 907–914, 2020.

[29] Q. C. H. L. Y. F. Lingyan GONG, Guangzhi LIAO, "Swollen Surfactant Micelles: Properties and Applications ," *Acta Physico-Chimica Sinica*, vol. 35, no. 8, pp. 816–828, 2019.

[30] B. P. Binks and S. O. Lumsdon, "Effects of oil type and aqueous phase composition on oil–water mixtures containing particles of intermediate hydrophobicity," *Physical Chemistry Chemical Physics*, vol. 2, pp. 2959–2967, 2000.

[31] D. J. M. Kuen Yong Lee, "Alginate: properties and biomedical applications," *Progress in Polymer Science*, vol. 37, no. 1, pp. 106–126, 2012.

[32] A. M. G.-C. S. B. T. N. H. L. N.-T. N. Zhuang Zhi Chong, Say Hwa Tan, "Alginate-Based Biomaterials for Regenerative Medicine Applications ," *Materials (Basel)*, vol. 16, no. 1, 2015.

[33] P. A.-E. Therese Andersen and M. Dornish

[34] T. N. Yingzhe Liu, Naotomo Tottori, "Microfluidic synthesis of highly spherical calcium alginate hydrogels based on external gelation using an emulsion reactant," *Sensors and Actuators B: Chemical*, vol. 283, pp. 802–809, 2019.

[35] A. I. B.-T. T. E.-S. C. Wan-Ping Voo, Chien-Wei Ooi, "Calcium alginate hydrogel beads with high stiffness and extended dissolution behaviour," *European Polymer Journal*, vol. 75, pp. 343–353, 2016.

[36] E. A. E. a.-E. K. S. M. B. F. M. T.-A. A. Farhad Abasalizadeh, Sevil Vaghefi Moghaddam, "Alginate-based hydrogels as drug delivery vehicles in cancer treatment and their applications in wound dressing and 3D bioprinting ," *Journal of Biological Engineering*, vol. 14, no. 8, pp. 2216—2230, 2020.

[37] M. S. M. F. K. H.M.C.De Azeredo, M.F.Rosa, "The use of biomass for packaging films and coatings ," *Advances in Biorefineries*, vol. 26, pp. 819–874, 2014.

[38] R. M. O. B. SilkeLorke, Uwe Müller, "Covalent cross-linking of polymers at room temperature ," *International Journal of Adhesion and Adhesives*, vol. 91, pp. 150—159, 2019.

[39] E. A. E. a.-E. K. S. M. B. F. M. T.-A. A. Farhad Abasalizadeh, Sevil Vaghefi Moghaddam, "Alginate-based hydrogels as drug delivery vehicles in cancer treatment and their applications in wound dressing and 3D bioprinting ," *Journal of Biological Engineering*, vol. 14, no. 8, 2020.

[40] H. P. S.-H. L. Sajjad Ashraf, Hun-Kuk Park, "Snapshot of Phase Transition in Thermoresponsive Hydrogel PNIPAM: Role in Drug Delivery and Tissue Engineering," *Macromolecular Research*, vol. 24, no. 4, pp. 297–304, 2016.

[41] Libretexts, "Free Radical Polymerization," 2020. `https://chem.libretexts.org/link?35129`, last accessed on 2020-12-05.

[42] D. W. Christopher D. Hein, Xin-Ming Liu, "Click Chemistry, a Powerful Tool for Pharmaceutical Sciences ," *Pharmaceutical Research*, vol. 25, no. 10, pp. 2216—2230, 2008.

[43] V. K. S. S. H.-S. S. N. M. Nidhi, Muzamil Rashid, "Microparticles as controlled drug delivery carrier for the treatment of ulcerative colitis: A brief review," *Saudi Pharmaceutical Journal*, vol. 24, no. 4, pp. 458–472, 2014.

[44] V. A. A. J. L. Miléna Lengyel, Nikolett Kállai-Szabó and I. Antal, "Microparticles, Microspheres, and Microcapsules for Advanced Drug Delivery," *Scientia Pharmaceutica*, vol. 87, 2019.

[45] J. S. A. S. J. Rathbone, *Fundamentals and Applications of Controlled Release Drug Delivery*. Springer, Boston, MA, 2012.

[46] S. H. I. Ramalingam Sitaraman and N. R. Kuloor, "A Generalized Equation for Diffusion in Liquids," *Indian Instit. Science*, vol. 8, no. 2, pp. 198–201, 1963.

[47] COMSOLAB, "COMSOL Multiphysics Handbook," 2009. `http://www.cntech.com.cn/down/h000/`, last accessed on 2020-12-05.

[48] COMSOLAB, 2009. `http://www.comsol.com.`, last accessed on 2020-12-05.

[49] Diener, “Activation with plasma ,” 2020. https://www.plasma.com/en/activation-with-plasma/, last accessed on 2020-14-04.